The source of A-type magmas in two contrasting settings: U–Pb, Lu–Hf and Re–Os isotopic constraints

The source of A-type magmas in two contrasting settings: U–Pb, Lu–Hf and Re–Os isotopic constraints.

[1]Pankhurst, M. J., [1]Schaefer, B. F., [1]Turner, S. P., Argles, T.[2], Wade, C. E.[3]

[1]GEMOC, Macquarie University, Sydney 2109, Australia

[2]Department of Earth and Environmental Sciences,

The Open University, Milton Keynes, MK7 6AA, UK

[3]Geological Survey of South Australia, Department for Manufacturing, Innovation, Trade, Resources and Energy (DMITRE), GPO Box 1264 Adelaide, South Australia, 5001

Corresponding author: Matthew J. Pankhurst matt.pankhurst@gmail.com

Keywords: Re–Os isotopes, A-type, U–Pb isotopes, Lu–Hf isotopes, post-orogenic, geodynamics, lithospheric stabilization.

Abstract: The source of post orogenic A-type magmas from two distinct geodynamic settings are compared. The end of the ca. 514 – 480 Ma Delamerian Orogeny, southeastern South Australia, was marked by ~10 Myr of bimodal A-type magmatism, driven by convective removal of thickened lithosphere. Initial Os and Hf isotope ratios record a heterogeneous lithospheric mantle source, with some input from aesthenospheric mantle. Mafic parental melts fractionated to produce the granites. In contrast, initial Os isotope ratios of the A-type magmas that comprise the ca. 1598 – 1583 Ma Mesoproterozoic Gawler Felsic Large Igneous Province, central South Australia, record a dominant evolved lower crust component. However, initial Hf isotope ratios from these samples are depleted, indicating a mantle source for lithophile elements. This voluminous, bimodal magmatism lasted for ~15 Myr, and ended the Wartakan Orogeny. In both cases the homogenisation of chemical (rheological) heterogeneities, inherited from terrain amalgamation and orogenic thickening, strengthened the lithosphere. The contemporaneous fusion of heterogeneous mantle ± crust may represent a common, stabilizing influence on the lithospheric column regardless of tectono-magmatic setting.

Introduction:

A-type magmas form a distinctive subset of igneous rocks. As a group, A-type granitoids are recognized as possessing a large number of mineralogical and geochemical affinities, that serve to clearly distinguish them from I- and S-type granitoids in the majority of cases (e.g. Collins et al., 1982). Importantly, their initial radiogenic isotope ratios are most often juvenile (e.g. Kemp et al., 2009; Turner et al., 1992), their temperatures high (e.g. King et al., 2001; Turner et al., 1992) and their emplacement depths shallow (Bonin, 2007). These features suggest a deep rooted mantle source region and influence of the magmatic system across the entire lithospheric column.

A-types granitoids (hereafter termed A-types) occur in a number of tectonic settings. First named as such by Loiselle and Wones (1979) due to their ‗anorogenic, anhydrous and alkalic' nature, A-types have subsequently been variably attributed to particular tectonic settings and melt source regions. Initially recognized as granites that occur along continental rift zones (Loiselle and Wones, 1979), A-types are also observed in post-collisional settings (Dargahi et al., 2010; Menuge et al., 2002) and as felsic portions of mafic large igneous provinces (e.g. Pankhurst et al., 2011a; Turner and Rushmer, 2009). Since A-types do not have one prevalent tectono-magmatic association (c.f. tholeiitic; mantle decompression melting, calc-alkaline; subduction zones), it is inappropriate to ascribe the mere presence of A-types to a single geodynamic setting.

An alternate approach is to use this apparently non-unique-setting magma type to highlight a potentially common influence upon the lithosphere, regardless of tectonic setting. Intriguingly, many A-type magmatic systems occur during the final stages of whichever tectono-magmatic expression they are a part of, and usually precede long periods of relative inactivity (e.g. Goodge and Vervoort, 2006; Puura and Flodén, 1999; Rämö and Haapala, 1995). Are A-types a cause, or effect, of a strengthened lithosphere? If a common influence is discovered, A-type magmas may have greater utility in geodynamic models.

It is widely accepted that rheological heterogeneity plays a fundamental role in determining the bulk strength of a lithospheric domain (e.g. Kelemen and Hirth, 2007; Paczkowski et al., 2012; Platt and Behr, 2011; Vissers et al., 1995). Often ‗runaway' deformation is observed (or modeled), which is focused within shear zones that

accommodate strain by grain size reduction and/or involvement of a liquid (melt) phase (e.g. Kelemen and Dick, 1995; Paczkowski et al., 2012; Sundberg et al., 2010). Chemical (and isotopic) heterogeneity is a product of such processes (e.g. Homburg et al., 2010), as well as metasomatic processes. Thus all else being equal, a chemically heterogeneous lithospheric domain is weaker than a chemically homogeneous domain (e.g. Vissers et al., 1995). Removing heterogeneity from a lithospheric domain is, by extension, a mechanism for lithospheric strengthening. In this contribution we explore the potential role that high temperature magmatism plays in homogenizing a lithospheric domain by causing widespread fusion of damaged, heterogeneous material and promoting pathways for mixing between distinct sources (homogenization). This post-orogenic re-organisation of high chemical (physical) gradients into low chemical gradients may serve to promote a stronger local lithosphere.

Should such magmatism play role in, or simply be a record of, lithospheric strengthening (and hence ―cratonisation‖), it is important to establish the ultimate source(s) and drivers of A-type provinces. These constraints can then be used to interrogate the geologic record in order to elucidate timing and duration of the onset of lithospheric stabilization. We explore the role of source in the petrogenesis of two adjacent, yet tectonically and temporally distinct A-type magmatic provinces from an isotopic perspective. Through a unique combination of Os and Hf isotopic techniques we evaluate the relative contributions of crust and mantle in the resultant granitoids and are able to highlight for the first time how a convergence of processes in the petrogenesis of these magmas can obscure some of the conventional isotopic signals relied upon in understanding the origin of these systems. We then comment on the implications of such magmatism in the formation of stable lithospheric columns and the preservation of continents.

Characteristics and petrogenesis of A-types

A-types most often display anhydrous mineralogy which is characterized by alkali feldspar + quartz > plagioclase > ferromagnesian + oxide minerals > accessory minerals (apatite, fluorite, zircon, titanite, other phosphates). A-types may display hypersolvus, transsolvus or subsolvus alkali feldspar (Bonin, 2007). Geochemical affinities include comparatively high Fe/Mg, (K+Na)/Al, Ga/Al and K/Na, elevated

rare earth and high field strength element (REE & HFSE) and F content, and light rare earth element (LREE) enrichment, resulting in ‗gull-wing' normalized REE patterns (e.g. Creaser et al., 1991; Whalen et al., 1987). They range from peraluminous to peralkaline to metaluminous, sometimes within a single province (e.g. Shellnutt and Zhou, 2007). Low O_2 fugacity and high temperatures up to ~1100 ºC (Frost and Frost, 1997; Whalen et al., 1987) are also common and important features.

Eby (1992) suggested that two groups of A-types are observed. A1 are those with element ratios similar to ocean island basalts (OIB), and form via crystal fractionation from melts of the same sources. A2 are those that display geochemical affinities with post-collisional continental or island arc crust, and have been suggested to form by partial melting of a previously I-type-granite-depleted lower crust (e.g. Clemens et al., 1986). However, Creaser et al. (1991) suggest this residual-source model is unlikely to account for all the mineralogical and geochemical observations. These authors demonstrated that A-types could be generated by partial melting of an undepleted, water poor crustal source with tonalitic-granodioritic composition. For a recent review of A-type petrogenesis, see Dall'Agnol et al. (2012).

Such geochemical variations within the group of granitoids termed ‗A-type' imply significantly different genesis in terms of their source, the degree of melting involved, and therefore thermal gradient. However, the most important factors in terms of physical properties of A-type felsic liquids; high temperature, alkali-rich major element chemistry, concentration of water (low) and halogens (high), are key characteristics of the group. Further, the corollary is that the material left behind during A-type extraction by either partial melting or fractionation will also bear a chemical resemblance to each other (Turner and Rushmer, 2009), which implies similar physical properties.

Importantly, the volume of material that is either cumulate or residue is also predicted to be relatively similar. For instance, Turner et al. (1992) modeled some A-types as the product of ~90% crystallization of a contemporary tholeiitic magma. The residual volume after extraction of an A-type liquid by partial melting is identical if the source is basaltic (Turner and Rushmer, 2009). Rocchi et al. (2009) estimated that ~20% partial melting of intrusive lamprophyres at the base of the crust could produce the observed A-types (albeit not strictly anhydrous in this example). In both instances the formation of a depleted mafic body at depth is implied. The key difference is that A-types formed by extreme (closed system) fractionation require a coeval volume of

mafic magma ~10x that of the granite volume. A-types formed by partial melting do not require large mafic magma chambers, as their source region could plausibly accumulate by iterative addition of small volume mafic melts.

Determining the source of A-type magmas

Radiogenic isotope ratios from A-types are most often juvenile (e.g. Kemp et al., 2009; Turner and Foden, 1996; Turner et al., 1992) —although not in every case (e.g. Huang et al., 2011)— and thus A-type magmas have been attributed with forming new granitic continental crust (c.f. recycling/maturation of older continental crust via I- and S- type magmatism; Villaseca et al., 2012). However, in many cases juvenile isotope ratios can also explained by the partial melting of juvenile crust and enriched mantle, and variable hybridization between these coeval magmas (e.g. Rutanen et al., 2010).

Traditional debate of A-types surrounds the role of mantle contributions to the crust over time, historically assessed by Nd-, and more recently Hf-isotope systems (e.g. Kemp et al., 2009). Both these systems reflect lithophile behaviour, but potentially may misrepresent a suspected mantle component, due to inheritance via magma assimilation or mingling (e.g. Pankhurst et al., 2011c). The Lu-Hf system broadly approximates the Sm-Nd, however due to the relative difference in D values, the Lu-Hf system is less affected by AFC processes (following the models of DePaolo, 1981). A distinct advantage for our purposes is that Hf in A-types (as in other granitoids) is primarily located within zircons. Thus inheritance of Hf can be clearly delineated through combined analysis with U-Pb geochronology. Zircons in granitoids contain Hf in concentrations of up to a few wt%, and contain comparatively little Lu (median = 150 ppm; Belousova et al., 2002) that would otherwise represent a source of uncertainty. Thus the initial Hf isotope ratio of the equilibrium liquid is preserved within magmatic zircon. Importantly, ingrowth of radiogenic Hf can be accurately age-corrected by U–Pb isotope analysis of the same region of zircon (Belousova et al., 2009).

A novel approach to the problem of A-type source regions is to utilise the Re-Os system. The ^{187}Re-^{187}Os decay scheme is most commonly used to inform siderophile and chalcophile element, and hence mantle, behaviour (e.g. Schaefer et al., 2010). However, very high Re/Os ratios in continental crust also make this system a very

sensitive monitor of crustal contributions to mantle derived magmas (e.g. Gregory et al., 2008; Shirey and Walker, 1998). For example, average continental crust is ~20 times more radiogenic than chondrite, and ancient lithospheric mantle contains sub-chondritic Os isotope ratios (Schaefer et al., 2000). A combined approach, using both Lu-Hf and Re-Os as a tool for mantle and crustal contributions to magmas, is underutilized despite this value (see Johnson et al., 1996).

Geologic Setting:

Undeformed plutons and associated volcanics of the Padthaway Ridge, southeastern South Australia, occur as an arcuate chain of A-type bodies that extends for ~300 km (Fig. 1a). These magmas represent the final tectono-thermal expression of the Delamerian Orogeny (~514-490 Ma; Foden et al., 2006), the first of a series of eastward-younging orogenies accreted to then Gondwanan margin, driven by a supra-subduction system (e.g. Kemp et al. 2009) The A-types are hypothesised to have formed when convective removal of overthickened lithospheric mantle led to rapid exhumation of the fold belt (Turner et al., 1996b). Post-convergent extension is argued to have allowed mafic melts to ascend to shallow depths, where closed-system crystal fractionation, involving olivine, pyroxenes, plagioclase and Fe-oxides took place (Turner et al., 1992), without significant crustal assimilation (Foden et al., 2002b). The predicted large volumes of intrusive mafic equivalents and cumulates are consistent with the presence of a gravity and aeromagnetic anomaly coincident with the Padthaway Ridge (e.g. Kennedy, 1989).

Immediately west of the rocks of the Delamerian Orogeny is the Tasman Line, a largely inferred lithospheric scale structure dividing western Precambrian Australia from the younger eastern basement successions (e.g. Arroucau et al., 2010). The closest occurrence of post-orogenic A-type magmatism in Proterozoic terranes west of the Tasman Line is that of the Hiltaba Event (1600-1560 Ma; Betts et al., 2002), which represents the last tectono-thermal episode of the central Gawler Craton (Fig. 1b) (Betts and Giles, 2006).

The Hiltaba Event is characterized by rapid, high temperature, voluminous and widespread bimodal A-type magmatism into and across a basement of Palaeoproterozoic and Archean rocks (Blissett et al., 1993; Pankhurst et al., 2011b). The voluminous Gawler Range Volcanics (GRV) were emplaced within 2 Myr at

1592 ± 2 Ma (Creaser, 1995; Fanning et al., 1988), extend for >25,000 km^2 (Blissett et al., 1993) and are overwhelmingly felsic (Allen et al., 2003). Basalts and basaltic andesites outcrop in just a few localities (Allen et al., 2008). Hiltaba Suite granitoids are considered the shallow intrusive equivalent to the GRV, crop out across much of the Gawler Craton, and span a longer time interval of emplacement, 1598 ±2 to 1583 ± 7 (Flint, 1993). These granites display a provinciality in terms of Nd isotopes (Creaser, 1995), which are suggestive of appreciable crustal involvement, supported by the observation of inherited zircon cores (e.g. Creaser and Fanning, 1993 and references therein).

Together the GRV and Hiltaba Suite Granitoids comprise the Gawler Felsic Large Igneous Province (FLIP). A large, elliptical, gravity high is coincident with the main GRV province (see data in Rajagopalan et al., 1993), which is consistent with significant volumes of mafic material predicted to exist at depth (Stewart, 1994). This anomaly was modeled by Phillips (2006) who filtered shallow sources and concluded the source of the gravity high was present at mid crustal levels.

The Gawler FLIP was preceded by ~10-20 Ma of crustal shortening, termed the Wartarkan Orogeny, that took place immediately after arc magmatism on the southern Gawler Craton margin ceased (Stewart and Betts, 2010b). The geometry of this arc-related calc-alkaline magmatism, and that of the Musgrave arc to the north, places the Gawler FLIP within a post-back-arc environment (Swain et al., 2008; Wade et al., 2006). Betts et al. (2009; 2007) used a synthesis of geologic, geochronological and geophysical data to propose a model that describes a plume head arrival as triggering the voluminous A-type magmatism, and progressed as hotspot-like magmatism across the eastern terranes of Proterozoic Australia. This plume-head-modified subduction was modeled by Betts et al. (2012), who found that the switching-off of subduction magmatism, and compression in the overriding plate, was likely due to trench advance, and not flat subduction. In their model, the buoyant plume head opened a window in the subducting slab, and was therefore able to interact with the overriding plate, without major reorganization of the subduction zone.

Samples and analytical techniques:

Samples

The Delamerian A-type system is represented in this dataset by two granites, (Marcollat and Seismograph), a rhyolite (Mt. Monster Porphyry), and a coeval peridotite cumulate (Black Hill peridotite), encompassing ~300 km of orogenic strike length, see figure 1a. Details of these samples can be found in Turner et al. (1992) and Turner, (1996). We also analysed a representative sample of the ca. 525 Ma Truro Volcanics, which are small volume strongly undersaturated alkali basalts that erupted immediately prior to the Delamerian Orogeny (see Forbes et al., 1972; Turner and Foden, 1990), for Re-Os. This allows a comparison to be made on the nature of the lithospheric mantle, in terms of Re-Os, before and after the orogeny.

The Gawler FLIP is represented by the most mafic portions of the GRV accessible. They are from across the central Gawler Craton, and provide a ~350 km wide footprint, to assess source homogeneity, see figure 1b. Samples are from Chitalinga Hill (a basaltic trachyandesite), White Hill (troctolite), and Roopena Volcanics (basalt and trachybasalt). We also analysed samples of the A-type ca. 1560 Ma Sybella Granite, Mt. Isa Inlier, Queensland Australia for Re-Os. This is considered a northern extension of the Mesoproterozoic hotspot trail (Betts et al., 2007), and allows us to compare Re-Os sources across the Proterozoic terranes of Australia.

In-situ zircon analysis

Zircon fragments and complete crystals up to ~210 µm from the Marcollat Granite (n=33) and Mount Monster Porphyry (n=35) were separated, hand picked, mounted in resin, and polished. The structure of the zircons were assessed by cathodoluminesence (CL) and back-scattered electron (BSE) imaging using a Cameca SX100 Electron Microprobe (EMP), which was also used to analyse ~1µm spots upon the grains for major elements, see figure 3.

A New Wave UP-213 laser ablation system (5 Hz repetition rate, 30 µm spot size, λ=213 nm) with a small format cell was used to ablate the grains, and an attached Agilent 7200 Series ICPMS measured trace element, U, Th and Pb isotope concentrations. After ≥60 s background count time, ablation intervals were 60-120 s per grain depending on the depth of available crystal. Several spots per single grain were analysed in order to explore any variation of age or trace elements within single grains. Marcollat (n=33) and Mt. Monster zircons (n=35) were analysed in one session each. The total of 72 analyses of unknowns were bracketed into six runs by

the isotopically homogeneous GEMOC-GJ-1 zircon standard (n=16), used to correct for U/Pb fractionation. For details of the GEMOC-GJ-1 standard see Elhlour et al. (2006). Two well-characterised zircons; 91500 (n=8) and Mud Tank (n=4) were analysed as independent controls on reproducibility and accuracy of isotope ratios; each returned an average within 2σ of the long-term $^{207}Pb/^{206}Pb$ ratio mean reported by Belousova et al. (2009). The data was processed using GLITTER software (www.glitter-gemoc.com) to calculate isotope ratios. The analytical procedures for the U–Pb dating are described in detail in Jackson et al. (2004). Analyses of the NIST-610 glass trace element standard (n=8) bracketed the analyses at regular intervals. Hf concentrations, measured by EMP, were used as known values with which to equate ICPMS total counts with concentration.

Hf, Lu and Yb isotopes were measured by a New Wave UP-266 laser ablation system (5 Hz repetition rate, 40 μm spot size) attached to a Nu-plasma multicollector ICP-MS. Typical ablation times were 100-120 s, and total Hf beams were between 1.5 and 3 V, depending on the structure and size of the zircon and Hf content. Detailed analytical procedures including corrections for mass interference can be found in Belousova et al. (2009). A single session for each of the sample was bracketed by four analyses of the Mud Tank zircon standard ($^{176}Hf/^{177}Hf$ = 0.282535 ±47, n = 12 and 0.282539 ±16, n=7 for the Marcollat Granite and Mount Monster respectively). In addition the Temora standard was used for Mount Monster ($^{176}Hf/^{177}Hf$ = 0.282732 ±39 n=7) and 91500 for the Marcollat ($^{176}Hf/^{177}Hf$ 0.282352 ±9, n = 1), all errors reported are 1σ. Care was taken to ablate spots immediately adjacent to U-Pb and trace element determinations, within the same CL imaged zone.

Whole rock Hf isotope analysis

A whole rock digestion for Hf isotope analysis for the Seismograph Rocks sample used standard HF-HNO_3 and purification was performed by standard anion exchange column separation techniques at the Geochemical Analysis Unit (GAU) of GEMOC, Macquarie University. The method was the same as that used for Gawler FLIP samples (Fricke, 2005). Hf isotope ratios were analysed by multi-collector ICP-MS (Nu plasma) also at the GAU and corrected to interpolated Lu and Hf values from Turner et al. (1992). BHVO-2 was used as an internal standard and returned a

$^{176}Hf/^{177}Hf$ ratio of 0.283089 ±18 (2σ). JMC475 was used as an external standard and returned a $^{176}Hf/^{177}Hf$ ratio of 0.282157 ±27 (2σ).

Whole rock Re–Os isotopic analysis

Re–Os methodology follows that of isotope dilution techniques described in Gregory et al. (2008). Whole-rock powders for each sample were spiked for Re and Os and digested in inverse aqua regia (8 ml 16N HNO_3, 4 ml 12N HCl) by carius tube dissolution followed by solvent extraction using the methods of Shirey and Walker (1995) and Cohen and Waters (1996) as described in Lambert et al. (1998, 2000). Rhenium was purified following Os extraction using anion exchange chromatography (Lambert et al. 1998). Osmium was analysed by N-TIMS on either a Thermo-Finnigan Triton at Macquarie University, Australia or at the Open University, UK. The Os samples were loaded onto Pt filaments and analysed using a combination of peak hopping or static collection depending on beam intensity for a minimum of 100 ratios and more typically 250.

Rhenium was determined using a Nu-Plasma multi-collector inductively coupled plasma mass spectrometer (MC-ICPMS) at the GAU or the Open University. A Re standard solution was analysed every five samples to monitor drift and fractionation. Mesoproterozoic samples were blank corrected using values of 1 pg Re and 1.4 pg Os with a $^{187}Os/^{188}Os$ ratio of 0.165 (GAU; as per Gregory et al., 2008). Delamerian data were blank corrected using 0.23 pg Os with a $^{187}Os/^{188}Os$ ratio of 0.2713 (Open University). This corresponds to corrections of up to 22% and 7%, respectively. Whole-rock standard (WPR-1) values averaged 10.8 ppb Re, 16.5 ppb Os with $^{187}Os/^{188}Os$ ratio of 0.14473, reproducing accepted values (e.g., Cohen and Waters 1996).

Results

In-situ U–Pb and Lu–Hf data from the Marcollat and Mt. Monster samples are presented in Table 1a and 1b respectively. In-situ trace element data from the Mt Monster zircons is also presented in Table 1b. For Marcollat zircon images, trace

element results and discussion see Pankhurst (2012). Whole rock Re–Os and Lu–Hf data, and a summary of the in-situ Lu-Hf data are presented in Table 3.

In situ zircon results

Strong oscillatory CL zoning is ubiquitous in the Marcollat Granite zircons (Fig. 2a), as is almost total absence of macro-inclusions, see Pankhurst (2012). Where geochronological information was obtained on both a core and rim, U–Pb ages are within error of each other, and common Pb correction was not required (Table 1a). The age of the Marcollat Granite is determined to be 480 ±2.5 Ma n=28 (Fig. 3a).

The Mount Monster Porphyry zircons typically have metamict and/or fractured cores and cleaner rims (Fig. 2b). The often complex fracturing resulted in U–Pb ages that are mostly discordant, probably due to a combination of both Pb-loss and presence of common Pb (Fig. 3b). The age of the Mt Monster Porphyry is determined to be 485.2 ±6.9 Ma n=11, the greater error reflecting the large number of discordant grains, which were discarded. One zircon core (rounded and non-metamict) from the Monster Porphyry returned a concordant age of 3034 ± 58 Ma. The individual age of the rim of this grain is 474 ± 10.9 Ma (concordant), which demonstrates that the presence of this Archean-aged zircon core is not a result of lab contamination.

The Mt. Monster zircons contain U, Th, Y, Hf and Yb abundances are typical of crustal granitoids (see Belousova et al., 2002). Rare earth elements vary by up to three orders of magnitude, La; 0.77-168 ppm, Ce; 3.8-1842 ppm, Pr; 0.37-58 ppm, Er; 3.3-2175 ppm, Tm; 3.4-496 ppm. The varying degree of fracturing and metamictisation most likely contributes to elevated REE (e.g. Belousova et al., 2006). Results of trace element abundances, including REE of the Marcollat zircons, are discussed in Pankhurst (2012). With the possible exception of Ti, trace elements do not correlate Hf isotope variation.

The Marcollat Granite zircon measured $^{176}Hf/^{177}Hf$ ratios range from 0.282554 to 0.282776, with an average of 0.282603 ± 0.000108 2σ. There is no correlation with $^{176}Yb/^{177}Hf$, which ranges from 0.03385 to an outlier of 0.1849, indicating the small corrections applied due to Yb interference on mass 176 are appropriate. The Mt. Monster zircon measured $^{176}Hf/^{177}Hf$ ratios range from 0.282525 to 0.282986, with an average of 0.282652 ± 0.000212 2σ. There is no correlation with $^{176}Yb/^{177}Hf$, which

ranges from 0.0393722 to an outlier at 0.252503, indicating these slightly larger corrections applied due to Yb interference are also appropriate.

The Marcollat zircons εHf_i, calculated using a ^{176}Lu decay constant of 1.93 $x10^{-11}$; Siguigna et al, (1982) from Blichert-Toft and Albarède (1997), range from +2.2 to +10.4, at 480 Ma. Mount Monster Porphyry zircon εHf_i ranges from +0.1 to +17.5, at 485 Ma. Both the Marcollat and Mt. Monster zircons are similarly aged, and contain a similar average and range of εHf_i values.

Whole rock Lu-Hf results

The Seismograph Granite has a $^{176}Hf/^{177}Hf$ ratio of 0.282701, and a $^{176}Lu/^{177}Hf$ ratio of 0.002310 (calculated from Turner et al. 1992 using reasonable Yb/Lu and Zr/Hf ratios in A-types, see Table 3), resulting in an εHf_i of 3.97. The Gawler FLIP samples measured $^{176}Hf/^{177}Hf$ ratios range from 0.282168 at Chitanilga Hill, to 0.282397 at Roopena, and correspond to εHf_i values of -1.73 and 4.95 respectively (Fricke, 2005).

Whole rock Re-Os results

$^{187}Os/^{188}Os_i$ for Delamerian samples ranges from 0.1051 to 0.1977. Compared with C1 chondrite and DMM at ca. 485 Ma, 0.124 and 0.121 respectively, these values range from sub- to slightly supra- chondritic. Intriguingly the highest $^{187}Os/^{188}Os_i$ value was from the most primitive sample: the Black Hill peridotite. The sample of Truro Volcanics yielded ratios of 0.1825 and 0.1875 and Os concentrations of 17.642 and 18.190 ppt in duplicate analyses respectively. The Black Hill Peridotite has the highest Os concentration of 405 ppt, while the granites have Os concentration of between 0.211 and 0.800 ppt.

Proterozoic samples have $^{187}Os/^{188}Os_i$ ratios that range from 0.9467 to 15.71, and Os concentrations range between 1.40 and 145 ppt, with no obvious correlation. A clear distinction is observed between Hiltaba A-types that exhibit radiogenic initial Os ratios and relatively high Os concentrations, and Delamerian A-types that exhibit unradiogenic initial Os ratios and low Os concentrations.

Discussion

New zircon ages

The Marcollat Granite age of 480 ± 2.5 Ma is slightly younger than Foden et al.'s (2006) 487.1 ± 1.2 Ma conventional single zircon age for the same granite. However, the Mount Monster Porphyry age of 485.2 ±6.9 Ma overlaps both. A single inherited concordant zircon dated at 3034 ±58 Ma represents the first Archean signal detected in the Delamerian granites. This grain was unlikely to have been assimilated near-surface, given the absence of an age peak in regional sedimentary zircon data (Ireland et al., 1998), thus we propose the existence of deep crustal Archean rocks, equivalent to the ~3.1 Ga Cooyerdoo Granite of the eastern Gawler Craton (Fraser et al., 2010) and/or Archean-derived rocks at significant depth. A single inherited concordant zircon is dated at 519 ±6 Ma, which may indicate the Marcollat Granite has interacted with Truro Volcanics aged material. However, significant crustal contamination to the granites is ruled out by Os isotope constraints, discussed in a later section.

Hf isotope constraints

The maximum recorded εHf_i of the Marcollat and Mt. Monster samples (+10.4 and +17.5) approach values for the contemporary depleted MORB mantle (DMM) (Fig. 4). The range (average +4.5, +5.7 respectively) is interpreted to be the result of complex magma mixing and mingling processes, which is reflected by the Seismograph Granite whole rock εHf_i of +3.97. Their source, therefore, is likely to be mantle, which accounts for the maximum values and also the prevalence of positive values approaching CHUR. However, the Hf isotope constraints alone do not rule out crustal contamination.

An additional constraint on the degree of crustal contamination in A-type magmas may be obtained following the approach of Heinonen et al. (2010). These authors linked magmatic cooling with assimilation of crustal material. Assimilation-related cooling was inferred by a correlation between decreasing Ti in zircons (lower temperature, lower Ti concentration; Watson et al., 2006) and less radiogenic Hf isotopes, as illustrated by figure 5. Assimilation of crust cools the magma, and by the same processes contributes relatively more-evolved Hf isotopic ratios. Zircons

crystallizing during the early stages of this process are predicted to contain relatively high Ti concentrations and high Hf isotope ratios. Assuming comparable Ti activity and an isotopically homogeneous assimilant, later zircons must contain relatively less Ti and lower Hf isotope ratios (see Fig. 5). In our samples, which have not interacted with crust (see discussion of Os isotopes below), this same approach can be used for a different purpose – to evaluate the range of initial Hf isotope ratios in the mantle source.

Absolute temperatures for our zircons were not calculated, as the Ti-in-zircon thermometer is calibrated assuming a rutile —and therefore Ti activity— buffer (Watson et al., 2006). Since rutile is not observed within the Marcollat or Mt. Monster samples, we use the measured Ti abundances as a relative guide only. We also include the caveat that Ti-bearing mineral inclusions within the zircons may introduce a degree of scatter. To minimise this effect close attention was paid to the signal quality, to identify spikes that may indicate the presence of an inclusion. However, evenly distributed micro-inclusions well below the scale of the laser-spot diameter may present an inherent source of uncertainty (see Pankhurst, 2012).

The Mt. Monster zircon population does not suggest a trend (see Fig. 5), and includes several outliers at high $^{176}Hf/^{177}Hf$. One interpretation is that these zircons crystallised ‗early', prior to crustal assimilation, which suggests the Hf isotope ratios are a robust reflection of a mantle source. However, these ‗early' zircons may have crystallised from a liquid that could have had different Ti activity. Therefore comparisons between Ti abundance in such zircons are problematic. A cluster of several analyses is present at high Ti contents, and may well indicate the presence of Ti-oxide micro-inclusions. Therefore we consider these Ti abundances to overestimate the real Ti content in the zircons.

Ti abundances in the Marcollat zircons show a broad positive correlation with measured $^{176}Hf/^{177}Hf$ (Fig. 5), which may indicate an assimilation process similar to that described by Heinonen et al. (2010). However, unlike Heinonen et al.'s (2010) data that define smooth trends, our data contain many instances of different $^{176}Hf/^{177}Hf$ at similar Ti abundance, as well as many instances of different Ti abundances with similar $^{176}Hf/^{177}Hf$. Notwithstanding the possibility of minor influences from Ti-oxide micro-inclusions, this observation could indicate that mixing of magmas with different cooling and assimilation histories, each contributed zircons that record those different magmatic conditions. Since the data in this study spans a

range in $^{176}Hf/^{177}Hf_i$ at comparable Ti concentrations, it would seem that no significant crustal involvement is implied from the Hf data.

Mingling of mafic and felsic magmas is observed within the Padthaway Suite — and indeed in many A-type magmatic systems— most evident where swarms of mafic enclaves occur within granites and show varying degrees of hybridisation (e.g. Holden et al., 1991; Turner and Foden, 1996). This causes additional complexities to the interpretation of whole-rock isotope ratios.

Pankhurst et al. (2011c) traced the sources of both mafic enclave and felsic host within the Delamerian A-type Mannum Granite by conducting in-situ analysis of Nd isotope ratios within titanite. Those authors demonstrated that while the major and trace element chemistry is distinct between granite-hosted and enclave-hosted titanite, isotope ratios are variable outside of analytical error, and the range of initial $^{143}Nd/^{144}Nd$ is similar. One possibility is that a range of sources melted to form geochemically similar, yet isotopically distinct mafic magmas.

The resulting magmas (containing isotopically distinct titanite crystals) were readily mixed due to similar viscosities. A similar process produced granites containing chemically similar yet isotopically dissimilar titanite crystals, which also mixed readily. Mingling occurred between the granite and mafic magmas due to different viscosities at comparable temperatures (Turner and Foden, 1996). This model, suggestive of complex, multi-sourced and multi-staged processes could plausibly result in a wide spread of initial $^{176}Hf/^{177}Hf$ values within zircons, dependent upon the source of melting, and crystallisation conditions each zircon.

Initial Hf isotope ratios from Gawler FLIP samples are range from -1.73 to +4.95. Crustal contamination is likely to play a limited role in contributing to these isotopic ratios, since the bulk rock compositions are relatively primitive (46.5 – 53.6 wt% SiO_2, 4.43 – 7.1 wt% MgO). The more mafic Gawler FLIP samples contain more evolved Hf isotope ratios, which suggest their source was also evolved (Fricke, 2005) relative to depleted mantle, consistent with a plume-like source (e.g. Nelson et al., 2012). These magmas are consistent with being derived from a plume source as implied by Betts et al. (2009), but could also originate from enriched lithospheric mantle, which could also explain their alkalic compositions and Hf isotope ratios ranging across CHUR.

The Hf isotope data from both the Delamerian and Gawler FLIP samples are suggestive of mantle sources. However, the Delamerian samples contain evidence of

appreciably depleted and juvenile material, which has likely mixed with relatively evolved material, either enriched lithospheric mantle or potentially crustal sources.

Os isotope constraints

Os isotopes are particularly distinctive between the A-type rocks of the Delamerian and Gawler FLIP (see Fig. 6). The $^{187}Os/^{188}Os_i$ of the Delamerian peridotite and felsic samples are extremely similar, and unradiogenic (Fig 6a). While their total Os concentrations range over 3 orders of magnitude (0.211 – 405 ppt), their $^{187}Os/^{188}Os_i$ have a comparatively narrow range from 0.1049 to 0.1977. The dramatic difference in Os concentration is consistent with the ~90% fractionation from a mafic mantle melt to produce the granitic compositions (Turner et al., 1992). The rhenium-depletion age of the most unradiogenic sample is 3.29 ± 0.4 Ga. The pre-Delamerian samples (Truro Volcanics) also contain relatively unradiogenic and homogeneous Os. $^{187}Os/^{188}Os_i$ range from 0.1825 – 0.1875 and concentrations between 1.7 – 1.8 ppt. These ratios are consistent with a weakly enriched lithospheric mantle source, supporting the conclusions of Turner et al. (1996a) and Foden et al. (2002a), who describe these HREE depleted, yet LREE enriched alkali basalts as originating from the upper lithospheric mantle.

Importantly, significant crustal contamination of the Delamerian magmas is ruled out by the Os data. The concentrations of Os are so low in the granites, that mixing with any reasonable average crustal component (Fig. 6a) will rapidly produce liquids that have both Os concentrations and $^{187}Os/^{188}Os_i$ significantly higher than measured in the Delamerian A-types. In fact, in order to be able to assimilate significant amounts of crust prior to closed system fractionation, any crustal component requires anomalously low levels of Os; of the order of sub ppt levels. The extremely low concentrations of Os and unradiogenic $^{187}Os/^{188}Os_i$ of the felsic samples support a petrogenesis dominated by closed system fractionation at high crustal levels, effectively bypassing an evolved lower crustal source.

Mt Monster is the only felsic sample which may contain up to a maximum of ~2% contamination (Fig. 6a) prior to fractionation, and intriguingly, this is the sample that contains the 3.1 Ga zircon core. The most radiogenic of the Delamerian samples is the Black Hill Peridotite, which on these models can be accounted for by assimilating a maximum of 5% crust. Since the Black Hill Peridotite is a significantly larger body

than the Marcollat and Seismograph Granites (Turner, 1996), it presumably spent more time at temperature in the crust, and therefore a greater degree of crustal assimilation is predicted.

Significantly, the other Delamerian samples are subchondritic, and therefore potentially record heterogeneities in the magma source. Such Os signatures are confined almost exclusively to the mantle, and therefore we interpret the primary magmatic source for the Delamerian A-types as the lithospheric mantle with only minor crustal modification. This is consistent with the conclusions of Foden et al. (2002b).

In contrast, the Gawler FLIP samples are highly variable and radiogenic ($^{187}Os/^{188}Os_i$ between 0.9467 and 15.71), and have less variable Os concentrations: between 11.8 and 145 ppt (Fig. 6b). These ratios clearly demonstrate the magmas‘ Os budget was derived from an ancient, evolved source. The high silica end of our Proterozoic A-type dataset, the Sybella Granite, also contains highly radiogenic Os ($^{187}Os/^{188}Os_i$ between 2.036 and 4.912), and contains comparatively little Os (1.4 – 1.7 ppt), consistent with fractionation from an Os source similar to that of the Gawler FLIP.

Since prevailing models for the Gawler FLIP invoke a mantle plume genesis (e.g. Betts et al., 2009), the Os isotopes point clearly towards assimilation of substantial amounts of continental crust into a plume derived magma. However, since the nature of the Archaean continental crust is poorly constrained, it is not yet possible to construct detailed models regarding the relative proportions of such crust. Since the lithophile isotopes (particularly Nd isotopes) do preserve evidence of a mantle-like component (Fricke, 2005), it is probable that the Os budget in the assimilated crust dominates any mantle signature.

Combined U–Pb, Lu–Hf and Re–Os constraints

Pankhurst et al. (2011c) found that multiple sources are required to account for the Nd isotopic variability within a Delamerian A-type granite exhibiting obvious mingling textures between host granite and mafic enclaves. In our Marcollat Granite- and Mt Monster Porphyry- examples that lack clear mingling textures, evidence for multiple sources is demonstrated by the large range of Hf isotope ratios within zircons. Thus multiple isotopic sources appear to be a feature of this system.

585 The U–Pb data implies a very low level of shallow crustal involvement since only
586 one of the 68 zircon grains analyzed in this study was clearly inherited, most likely
587 from a lower crustal source. In addition, the Os isotope data effectively rules out
588 significant crustal contamination, especially of granites whose Os concentrations are
589 extremely sensitive to any external source Os.
590 Initial Hf isotope data contains examples of DMM-like ratios, although most
591 examples are less radiogenic (Fig. 4). Importantly, none are less radiogenic than
592 CHUR. The spread of initial Hf isotope values appear to be unrelated to
593 straightforward assimilation of cooler, evolved material (Fig. 5), and since the Os data
594 rules out crustal contamination (Fig. 6a), this spread is most likely to reflect mantle
595 source heterogeneity.
596 The sub-chondritic Os values must reflect a lithospheric mantle source, since
597 contemporary DMM is more radiogenic (see Fig. 6a). The significant heterogeneity of
598 the source, as required by the spread of Hf data on the positive side of CHUR (Fig. 4),
599 must therefore have been within the lithospheric mantle. Thus a source dominated by
600 material from heterogeneous lithospheric mantle is constrained by the combination of
601 lithophile and chalcophile systems within the Delamerian A-types.
602 The rarity of DMM-like Hf isotope ratios recorded by zircons, and the sub-
603 chondritic Os isotope ratios argue strongly for a dominant lithospheric mantle source.
604 The range in both Hf and Os isotope ratios are consistent with a variably enriched and
605 heterogeneous lithospheric mantle, potentially due to metasomatic processes during
606 the preceding orogenesis. This interpretation is consistent with both Turner et al.
607 (1992) and Foden et al. (2002b) who also invoked a metasomatised lithospheric
608 mantle source for the Delamerian A-types on the basis of major and trace element and
609 Sr and Nd isotope constraints.
610 Initial Hf isotope ratios from the Gawler FLIP samples are similar to those of the
611 Delamerian, as they cluster at the radiogenic side of CHUR. In terms of lithophile
612 elements, both the Gawler FLIP and the Delamerian A-types point to a dominant
613 mantle component. Such a source for the Gawler province has been suggested on the
614 basis of high magmatic temperatures (950-1100 °C) and Nd isotopes (Stewart and
615 Foden, 2001). However, distinct provinciality, reflecting variable and significant
616 assimilation of crust on a pluton scale has been described (e.g. Swain et al., 2005). In
617 support of a significant crustal contribution, the initial Os isotope ratios are extremely

radiogenic, which can only be reasonably attributed to the involvement of an ancient, evolved source (Fig. 6b). Assimilation or melting of Archean crust is one possible explanation, supported by the recent discovery of gneissic Archean granites within the Gawler Craton (Fraser et al., 2010). Another possibility is the involvement of metasomatised, highly radiogenic portions of the source region. In either scenario, it is clear that the Os budget of the Gawler samples are not dominated by an aesthenospheric mantle signature.

Do A-type magmas play a role in strengthening lithosphere?

Granitic magmatism plays an important role in the distribution of heat-producing elements in the lithosphere, and long-term stability of crustal domains (Sandiford and McLaren, 2005). The observation that A-type magmas are virtually always post-kinematic invites speculation as to whether there exists a genetic link between the end of orogenesis and A-type magmatism on shorter time frames as well. Since the majority of these post-orogenic magmas remain undeformed, this suggests their presence within stable crustal domains is not a coincidence. Rather their presence may be reflective of a strengthening process that either drives or is driven by A-type magmatism. Removal of heat-producing elements from lithospheric mantle sources via A-type magmatism may promote the longer-term strength and thus stability of those source regions.

For instance, Puura and Flodén (1999) describe the well-studied 1.65-1.50 Ga rapakivi magmatism of the Svecofennian Domain as being directly related to crust thickened by the ~300 Ma older Svecofennian Orogeny. This gravitationally unstable crust is the driver of mantle diapirism, which causes major crust and mantle melting, producing the A-type magmas. The magmatism effectively stabilizes the lithospheric column by resetting the Moho depth and thinning the crust (Puura and Flodén, 1999).

Another well-documented example is the Tasmanide orogenies of eastern Australia, beginning with the Delamerian. A series of eastward-younging orogenies accreted to then Gondwanan margin, driven by a supra-subduction system. Within this cyclical amalgamation of continental mass, pulses of mantle input over time are recorded by positive excursions of Hf and Nd isotope ratios (e.g. DeCelles et al., 2009) via A-type magmatism that post-date peak deformation of each orogeny (Kemp et al., 2009). This contrasts with negative Hf and Nd excursions of the syn-orogenic I-

and S-type granite record (Kemp et al., 2009). These observations imply the same process occurred to terminate each of these Phanerozoic orogenies, and promoted later deformation outboard to continue the cycle. We have progressed the work of Kemp et al. (2009) to include the Delamerian A-types. Our data definitively establish that the source of these magmas is a heterogeneous lithospheric mantle. Whole-rock Os isotope data from the A-types of the subsequent Tasminides would serve as an authoritative test of whether the same sources were melting at the closing stages of each orogeny, and therefore the same processes were operating to terminate each orogeny.

Our isotopic evidence from the Delamerian suggests that a heterogeneous lithospheric mantle was the most important source of the magmas. The magmatic system produced high-crustal level granites that were ultimately sourced from various portions of the underlying mantle, representing a significant homogenizing influence across the lithospheric column. This process may have been driven by convective removal of orogenic-thickened lithosphere (Turner et al., 1996b), which represents a fundamental change in the orogenic stress field, terminating the Delamerian Orogeny. We suggest that the homogenizing influence of the A-type magmatic system promoted, and potentially drove, local strengthening of this lithosphere via chemical and therefore physical reorganization/resetting, which directed future deformation outboard.

The decoupling of the Hf and Os isotope systems implies the Gawler FLIP was produced from a number of sources. Radiogenic initial Nd and Hf isotope ratios strongly argue for a mantle source, which is consistent with the prevailing plume-head-arrival model for the province as a whole (Betts et al., 2009). However, an evolved source must also contribute significant material in order to dominate the Os budget, which is consistent with the observed skewing of Hf isotope values towards CHUR. Future work characterizing the Os isotope signature of Gawler Craton crustal rocks is required to constrain whether the source of the radiogenic Os is crustal, or can be attributed to highly metasomatised portions of the lithospheric mantle. This determination has implications for the degree of source heterogeneity within the Gawler FLIP. In either case, the source of Os is clearly different from that of the Delamerian samples.

The Gawler FLIP contains both mantle and crustal isotopic signatures, which points to a significant depth range of melting and operation of the magmatic system.

The voluminous, high temperature and rapid nature of the GRV emplacement points to wholescale melting of the fusible portions of the lithospheric column, effectively homogenizing pre-existing chemical gradients. This, hypothesized, widespread ‗resetting' of rheological properties via the A-type magmatism could cause relatively strengthening of the lithospheric domain, which explains its position as an enduring stable block today.

Conclusions

The Delamerian and Gawler FLIP A-type systems have numerous similarities. They share distinctive chemistry and produce bimodal provinces characterized by high temperature (≤ 1100º C) shallow granites and rheoignimbrites/lavas and mid-crustal mafic intrusions. They both define 1) transient periods of anomalous thermal gradients, 2) the terminus of their respective orogenies (Delamerian, Wartakan), and 3) have occupied stable lithospheric blocks since. These observations suggest a common tectono-magmatic process.

There are also important differences. The Delamerian system has a comparatively small total volume, and its architecture is relatively long and narrow. The Gawler FLIP has a large total volume, and its architecture is elliptical. These features, independent of chemistry or source, are consistent with normal supra-subduction zone dynamics producing the Delamerian Orogeny (Kemp et al., 2009), and plume head involvement in the Gawler FLIP (Betts et al., 2009).

Our Hf and Os measurements constrain the dominant source regions of each. The Delamerian is appreciably depleted, containing DMM like Hf isotope ratios as well as Os isotope evidence of a lithospheric mantle source. Assimilation of continental crust plays a minor role, leaving a dominant portion of the signal attributed to heterogeneous lithospheric mantle. Critically, it is the combined approach of in-situ Hf analysis and whole rock Os analysis that allow us to confidently rule out crustal contamination, and instead attribute the range of Hf isotope ratios to be truly reflective of a heterogeneous lithospheric mantle source.

The Gawler FLIP is similarly juvenile in terms of Hf, yet much more evolved in terms of Os. Partial melting in an ancient lower crust is one explanation for the extremely radiogenic $^{187}Os/^{188}Os_i$, although metasomatised portions of a mantle source may also satisfy the data. Our isotopic data is consistent with widespread

melting and significant transfer of material from mantle to crust, caused by the arrival of a mantle plume head.

We observe the same style of magmatism, range of sources and empirical observation of a stable post-magmatic lithosphere in both the Delamerian and Gawler FLIP. The geodynamic end-member examples presented here (convective thinning/plume head arrival) suggest the spectrum of A-type magmatism is indicative of similar high temperature regimes, which can lead to the strengthening of lithosphere. If the thermal regime is adequately persistent, coeval fusion of crust and mantle, resetting of the moho, and removal of heterogeneities is suggested to promote long-term stability of lithospheric domains.

Acknowledgements

Elena Belousova, Will Powell and Rosanna Murphy are thanked for discussions of the manuscript. Peter Wieland is thanked for laboratory assistance. Bernard Bonin and an anonymous reviewer are thanked for their constructive comments which improved the manuscript. MJP would like to thank Karin Barovich, John Clemens and Nigel Harris for their comments on this manuscript within his PhD thesis. David Hilton is thanked for his editorial role.

Figure captions:

Figure 1. Location and geologic context of samples. a) The Padthaway Suite extends for ~500 km in a north-northwest direction, parallel with the coastline of southeast South Australia. The intrusions are exposed by the unroofing of Delamerian orogenic rocks since ~480 Ma. b) The Gawler Craton, central South Australia, is comprised of amalgamated Archean, Palaeo- and Mesoproterozoic terranes. The Gawler FLIP (Allen et al., 2008) represents the final tectono-magmatic event in the central Gawler Craton, before tectonic and magmatic activity continued on the northern margin (Stewart and Betts, 2010a).

Figure 2. Cathodoluminesence images of zircons and analytical spots in this study. a) Marcollat, b) Mt. Monster Porphyry.

Figure 3. Age concordia from selected analyses of the a) the Marcollat Granite and b) the Mt. Monster Porphyry. Discordant data (filled, greyed) were rejected from age calculations.

Figure 4. Initial Hf isotope ratios for the Delamerian and Gawler FLIP magmatic rocks with respect to emplacement age. In both provinces the initial Hf isotope ratios are more juvenile than CHUR, and a small number of zircons from the Mt. Monster Porphyry are similar to contemporary DMM. Error bars are smaller than the lines displayed.

Figure 5. Measured $^{176}Hf/^{177}Hf$ ratios with respect to Ti concentration. As the Ti-in-zicron thermobarometer is calibrated using a rutile (and therefore Ti activity) buffer, and no rutile is observed within the Marcollat Granite or Mt. Monster Porphyry, we present Ti concentration as a temperature proxy only. Despite scatter due to probable micro-inclusions of Ti-oxides, a cooling trend can be observed within the Marcollat data (dashed lines). Mt. Monster Porphyry data is much more scattered and do not show a meaningful trend. [1]Zircon data from a biotite granite and a diabase within a comparable A-type system (Heinonen et al., 2010) are plotted for comparison. Symbol size is generally larger than the plotted error.

Figure 6. Initial $^{187}Os/^{188}Os$ ratios against inverse of Os concentration. a) Delamerian samples occupy a limited range from subchondritic to suprachondritic. The ratios cannot be explained by crustal assimilation, since mixing between a 10% partial melt of a DMM source (calculated following the approach of Roy-Barman and Allègre, 1995) and an average crustal component (Os concentration of 100-50 ppt and a $^{187}Os/^{188}Os$ ratio of 10) i) trend to far more radiogenic values than those measured and ii) do not approach the extremely low concentrations of Os measured. The data are best explained by closed system fractionation from a depleted lithospheric mantle source. b) The highly radiogenic values displayed by the Proterozoic samples are similar to a range of reasonable 3.1 Ga Archean Crustal values, which suggests mixing between mantle plume components and these ancient rocks could explain our data. Another possibility is that the high $^{187}Os/^{188}Os$ is due to high Re/Os metasomatic agents (such as subduction fluids; Widom et al., 1999) present in the source. Future

788 work constraining the Re and Os signature of Gawler basement rocks will allow
789 meaningful tests of these hypotheses. Error bars are smaller than the symbol size.
790
791 **References**
792

793 Allen, S. R., McPhie, J., Ferris, G., and Simpson, C., 2008, Evolution and architecture
794 of a large felsic Igneous Province in western Laurentia: The 1.6 Ga Gawler
795 Range Volcanics, South Australia: Journal of Volcanology and Geothermal
796 Research, v. 172, no. 1-2, p. 132-147.
797 Allen, S. R., Simpson, C. J., McPhie, J., and Daly, S. J., 2003, Stratigraphy,
798 distribution and geochemistry of widespread felsic volcanic units in the
799 Mesoproterozoic Gawler Range Volcanics, South Australia: Australian
800 Journal of Earth Sciences, v. 50, no. 1, p. 97-112.
801 Arroucau, P., Rawlinson, N., and Sambridge, M., 2010, New insight into Cainozoic
802 sedimentary basins and Palaeozoic suture zones in southeast Australia from
803 ambient noise surface wave tomography: Geophys. Res. Lett., v. 37, p.
804 L07303.
805 Belousova, E., Griffin, W. L., O'Reilly, S. Y., and Fisher, N. I., 2002, Igneous zircon:
806 trace element composition as an indicator of source rock type: Contributions
807 to Mineralogy and Petrology, v. 143, no. 5, p. 602-622.
808 Belousova, E. A., Griffin, W. L., and O'Reilly, S. Y., 2006, Zircon Crystal
809 Morphology, Trace Element Signatures and Hf Isotope Composition as a Tool
810 for Petrogenetic Modelling: Examples From Eastern Australian Granitoids:
811 Journal of Petrology, v. 47, no. 2, p. 329-353.
812 Belousova, E. A., Reid, A. J., Griffin, W. L., and O'Reilly, S. Y., 2009, Rejuvenation
813 vs. recycling of Archean crust in the Gawler Craton, South Australia:
814 Evidence from U-Pb and Hf isotopes in detrital zircon: Lithos, v. 113, no. 3-4,
815 p. 570-582.
816 Betts, P. G., and Giles, D., 2006, The 1800-1100 Ma tectonic evolution of Australia:
817 Precambrian Research, v. 144, p. 92-125.
818 Betts, P. G., Giles, D., Foden, J., Schaefer, B. F., Mark, G., Pankhurst, M. J., Forbes,
819 C. J., Williams, H. A., Chalmers, N. C., and Hills, Q., 2009, Mesoproterozoic
820 plume-modified orogenesis in eastern Precambrian Australia: Tectonics, v. 28,
821 p. Tc3006.
822 Betts, P. G., Giles, D., Lister, G. S., and Frick, L. R., 2002, Evolution of the
823 Australian lithosphere: Australian Journal of Earth Sciences, v. 49, no. 4, p.
824 661-695.
825 Betts, P. G., Giles, D., Schaefer, B. F., and Mark, G., 2007, 1600–1500 Ma hotspot
826 track in eastern Australia: implications for Mesoproterozoic continental
827 reconstructions: Terra Nova, v. 19, no. 6, p. 496-501.
828 Betts, P. G., Mason, W. G., and Moresi, L., 2012, The influence of a mantle plume
829 head on the dynamics of a retreating subduction zone: Geology, v. 40, no. 8, p.
830 739-742.
831 Blichert-Toft, J., and Albarède, F., 1997, The Lu-Hf isotope geochemistry of
832 chondrites and the evolution of the mantle-crust system: Earth and Planetary
833 Science Letters, v. 148, no. 1,Äì2, p. 243-258.
834 Blissett, A. H., Creaser, R. A., Daly, S. J., Flint, R. B., and Parker, A. J., 1993,
835 Gawler Range Volcanics, *in* Drexel, J. F., Preiss, W. V., and Parker, A. J.,

836 eds., The geology of South Australia, Volume 1: The Precambrian: Adelaide,
837 Department of Mines and Energy, p. 106-124.
838 Bonin, B., 2007, A-type granites and related rocks: Evolution of a concept, problems
839 and prospects: Lithos, v. 97, no. 1-2, p. 1-29.
840 Clemens, J. D., Holloway, J. R., and White, A. J. R., 1986, Origin of an A-type
841 granite; experimental constraints: American Mineralogist, v. 71, no. 3-4, p.
842 317-324.
843 Collins, W., Beams, S., White, A., and Chappell, B., 1982, Nature and origin of A-
844 type granites with particular reference to southeastern Australia: Contributions
845 to Mineralogy and Petrology, v. 80, no. 2, p. 189-200.
846 Creaser, R. A., 1995, Neodymium isotopic constraints for the origin of
847 Mesoproterozoic silicic magmatism, Gawler Craton, South Australia.:
848 Canadian Journal of Earth Sciences, v. 32, p. 469-471.
849 Creaser, R. A., and Fanning, C. M., 1993, A U-Pb Zircon Study of the
850 Mesoproterozoic Charleston Granite, Gawler Craton, South-Australia:
851 Australian Journal of Earth Sciences, v. 40, no. 6, p. 519-526.
852 Creaser, R. A., Price, R. C., and Wormald, R. J., 1991, A-type granites revisited:
853 Assessment of a residual-source model: Geology, v. 19, no. 2, p. 163-166.
854 Dall'Agnol, R., Frost, C. D., and Rämö, O. T., 2012, IGCP Project 510 "A-type
855 Granites and Related Rocks through Time" Project vita, results, and
856 contribution to granite research: Lithos, v. 151, no. 0, p. 1-16.
857 Dargahi, S., Arvin, M., Pan, Y. M., and Babaei, A., 2010, Petrogenesis of post-
858 collisional A-type granitoids from the Urumieh-Dokhtar magmatic
859 assemblage, Southwestern Kerman, Iran: Constraints on the Arabian-Eurasian
860 continental collision: Lithos, v. 115, no. 1-4, p. 190-204.
861 DeCelles, P. G., Ducea, M. N., Kapp, P., and Zandt, G., 2009, Cyclicity in Cordilleran
862 orogenic systems: Nature Geoscience, v. 2, no. 4, p. 251-257.
863 DePaolo, D. J., 1981, Trace element and isotopic effects of combined wallrock
864 assimilation and fractional crystallization: Earth and Planetary Science Letters,
865 v. 53, no. 2, p. 189-202.
866 Eby, G. N., 1992, Chemical subdivision of the A-type granitoids:Petrogenetic and
867 tectonic implications: Geology, v. 20, no. 7, p. 641-644.
868 Elhlou, S., Belousova, E. A., Griffin, W. L., Pearson, N. J., and O'Reilly, S. Y., 2006,
869 Trace element and isotopic composition of GJ red zircon standard by laser
870 ablation: Geochimica et Cosmochimica Acta, v. 70, no. 18, p. A158.
871 Fanning, C. M., Flint, R. B., Parker, A. J., Ludwig, K. R., and Blissett, A. H., 1988,
872 Refined Proterozoic evolution of the Gawler Craton, South Australia, through
873 U-Pb zircon geochronology: Precambrian Research, v. 40-41, p. 363-386.
874 Flint, R. B., 1993, Mesoproterozoic, *in* Drexel, J. F., Preiss, W. V., and Parker, A. J.,
875 eds., The Geology of South Australia, vol. 1: The Precambrian, Volume
876 Bulletin 54, Geol. Surv. South Australia, p. 107-169.
877 Foden, J., Elburg, M. A., Dougherty-Page, J., and Burtt, A., 2006, The Timing and
878 Duration of the Delamerian Orogeny: Correlation with the Ross Orogen and
879 Implications for Gondwana Assembly: The Journal of Geology, v. 114, no. 2,
880 p. 189-210.
881 Foden, J., Song, S. H., Turner, S., Elburg, M., Smith, P. B., Van der Steldt, B., and
882 Van Penglis, D., 2002a, Geochemical evolution of lithospheric mantle beneath
883 S.E. South Australia: Chemical Geology, v. 182, no. 2-4, p. 663-695.

884 Foden, J. D., Elburg, M. A., Turner, S. P., Sandiford, M., O'Callaghan, J., and
885 Mitchell, S., 2002b, Granite production in the Delamerian Orogen, South
886 Australia: Journal of the Geological Society, v. 159, p. 557-575.
887 Forbes, B. G., Coates, R. P., and Daily, B., 1972, Truro Volcanics: Quarterly
888 geological notes. Geol. Surv. South Aust., v. 44, p. 1-5.
889 Fraser, G., McAvaney, S., Neumann, N., Szpunar, M., and Reid, A., 2010, Discovery
890 of early Mesoarchean crust in the eastern Gawler Craton, South Australia:
891 Precambrian Research, v. 179, no. 1,Äì4, p. 1-21.
892 Fricke, C., 2005, Source and origin of the lower Gawler Range Volcanics, (GRV),
893 South Australia: geochemical constraints from mafic magmas., Monash
894 University.
895 Frost, A. M., 2009, Petrogenesis, Modelling and Characterisation of Layered Mafic
896 Intrusion White Hill and Peculiar Knob North within the Mount Woods Inlier,
897 South Australia [Honours: Macquarie University.
898 Frost, C. D., and Frost, B. R., 1997, Reduced rapakivi-type granites: The tholeiite
899 connection: Geology, v. 25, no. 7, p. 647-650.
900 Goodge, J. W., and Vervoort, J. D., 2006, Origin of Mesoproterozoic A-type granites
901 in Laurentia: Hf isotope evidence: Earth and Planetary Science Letters, v. 243,
902 p. 711-731.
903 Gregory, M. J., Schaefer, B. F., Keays, R. R., and Wilde, A. R., 2008, Re-Os
904 systematics of the Mt Isa copper ore body and the Eastern Creek Volcanics,
905 Queensland, Australia: Mineralium Deposita, v. 43, p. 553-573.
906 Heinonen, A. P., Andersen, T., and Rämö, O. T., 2010, Re-evaluation of Rapakivi
907 Petrogenesis: Source Constraints from the Hf Isotope Composition of Zircon
908 in the Rapakivi Granites and Associated Mafic Rocks of Southern Finland:
909 Journal of Petrology, v. 51, no. 8, p. 1687-1709.
910 Holden, P., Halliday, A. N., Stephens, W. E., and Henney, P. J., 1991, Chemical and
911 Isotopic Evidence for Major Mass-Transfer between Mafic Enclaves and
912 Felsic Magma: Chemical Geology, v. 92, no. 1-3, p. 135-152.
913 Homburg, J. M., Hirth, G., and Kelemen, P. B., 2010, Investigation of the strength
914 contrast at the Moho: A case study from the Oman Ophiolite: Geology, v. 38,
915 no. 8, p. 679-682.
916 Huang, H.-Q., Li, X.-H., Li, W.-X., and Li, Z.-X., 2011, Formation of high $\delta^{18}O$
917 fayalite-bearing A-type granite by high-temperature melting of granulitic
918 metasedimentary rocks, southern China: Geology, v. 39, no. 10, p. 903-906.
919 Ireland, T. R., Flöttmann, T., Fanning, C. M., Gibson, G. M., and Preiss, W. V., 1998,
920 Development of the early Paleozoic Pacific margin of Gondwana from
921 detrital-zircon ages across the Delamerian orogen: Geology, v. 26, no. 3, p.
922 243-246.
923 Jackson, S. E., Pearson, N. J., Griffin, W. L., and Belousova, E. A., 2004, The
924 application of laser ablation-inductively coupled plasma-mass spectrometry to
925 in situ U-Pb zircon geochronology: Chemical Geology, v. 211, no. 1-2, p. 47-
926 69.
927 Johnson, C. M., Shirey, S. B., and Barovich, K. M., 1996, New approaches to crustal
928 evolution studies and the origin of granitic rocks: what can the Lu-Hf and Re-
929 Os isotope systems tell us?: Earth and Environmental Science Transactions of
930 the Royal Society of Edinburgh, v. 87, no. 1-2, p. 339-352.
931 Kelemen, P. B., and Dick, H. J. B., 1995, Focused melt flow and localized
932 deformation in the upper mantle: Juxtaposition of replacive dunite and ductile

shear zones in the Josephine peridotite, SW Oregon: Journal of Geophysical Research, v. 100, no. B1.
Kelemen, P. B., and Hirth, G., 2007, A periodic shear-heating mechanism for intermediate-depth earthquakes in the mantle: Nature, v. 446, p. 787-790.
Kemp, A. I. S., Hawkesworth, C. J., Collins, W. J., Gray, C. M., and Blevin, P. L., 2009, Isotopic evidence for rapid continental growth in an extensional accretionary orogen: The Tasmanides, eastern Australia: Earth and Planetary Science Letters, v. 284, no. 3,Äì4, p. 455-466.
Kennedy, R. J., 1989, A 3D gravity and aeromagnetic interpretation of the Black Hill-Cambrai Region [Honours: University of Adelaide.
King, P. L., Chappell, B. W., Allen, C. M., and White, A. J. R., 2001, Are A-type granites the high-temperature felsic granites? Evidence from fractionated granites of the Wangrah Suite: Australian Journal of Earth Sciences, v. 48, no. 4, p. 501-514.
Loiselle, M. C., and Wones, D. R., Characteristics and origin of anorgenic granites, *in* Proceedings Geol Soc Am Abstr with Progr1979, Volume 11, p. 468.
Menuge, J. F., Brewer, T. S., and Seeger, C. M., 2002, Petrogenesis of metaluminous A-type rhyolites from the St Francois Mountains, Missouri and the Mesoproterozoic evolution of the southern Laurentian margin: Precambrian Research, v. 113, no. 3-4, p. 269-291.
Nelson, W. R., Furman, T., van Keken, P. E., Shirey, S. B., and Hanan, B. B., 2012, OsHf isotopic insight into mantle plume dynamics beneath the East African Rift System: Chemical Geology, v. 320–321, no. 0, p. 66-79.
Paczkowski, K., Bercovici, D., Landuyt, W., and Brandon, M. T., 2012, Drip instabilities of continental lithosphere: acceleration and entrainment by damage: Geophysical Journal International, v. 189, no. 2, p. 717-729.
Pankhurst, M. J., 2012, Determining the source of post-orogenic magmatism to constrain terminal orogenesis. [PhD (unpublished): Macquarie University.
Pankhurst, M. J., Schaefer, B. F., and Betts, P. G., 2011a, Geodynamics of rapid voluminous felsic magmatism through time: Lithos, v. 123, p. 92-101.
Pankhurst, M. J., Schaefer, B. F., Betts, P. G., Phillips, N., and Hand, M., 2011b, A Mesoproterozoic continental flood rhyolite province, the Gawler Ranges, Australia: the end member example of the Large Igneous Province clan: Solid Earth, v. 2, p. 1-9.
Pankhurst, M. J., Vernon, R. H., Turner, S. P., Schaefer, B. F., and Foden, J., 2011c, Contrasting Sr and Nd isotopic behaviour during magma mingling; new insights from the Mannum A-type granite: Lithos, v. 126, p. 135-146.
Phillips, N., 2006, Geophysical modeling of the Hutchison Group beneath the Gawler Range Volcanics, Gawler Craton, South Australia [Honours: Monash University.
Platt, J. P., and Behr, W. M., 2011, Grainsize evolution in ductile shear zones: Implications for strain localization and the strength of the lithosphere: Journal of Structural Geology, v. 33, no. 4, p. 537-550.
Puura, V., and Flodén, T., 1999, Rapakivi-granite-anorthosite magmatism - a way of thinning and stabilisation of the Svecofennian crust, Baltic Sea Basin: Tectonophysics, v. 305, no. 1-3, p. 75-92.
Rajagopalan, S., Zhiqun, S., and Major, R., 1993, Geophysical investigations of volcanic terrains: A case history from the Gawler Range Volcanic Province, South Australia: Exploration Geophysics, v. 24, p. 769-778.

Rämö, O. T., and Haapala, I., 1995, One hundred years of rapakivi granite: Mineralogy and Petrology, v. 52, no. 3-4, p. 129-185.
Rocchi, S., Di Vincenzo, G., Ghezzo, C., and Nardini, I., 2009, Granite-lamprophyre connection in the latest stages of the early Paleozoic Ross Orogeny (Victoria Land, Antarctica): Bulletin of the Geological Society of America, v. 121, no. 5-6, p. 801-819.
Roy-Barman, M., and Allègre, C. J., 1995, $^{187}Os/^{186}Os$ in oceanic island basalts: tracing oceanic crust recycling in the mantle: Earth and Planetary Science Letters, v. 129, no. 1,Äì4, p. 145-161.
Rutanen, H., Andersson, U. B., Väisänen, M., Johansson, A., Fröjdö, S., Lahaye, Y., and Eklund, O., 2010, 1.8 Ga magmatism in southern Finland: strongly enriched mantle and juvenile crustal sources in a post-collisional setting: International Geology Review, v. 53, no. 14, p. 1622-1683.
Sandiford, M., and McLaren, S., 2005, Thermo-mechanical controls on heat production element distributions and the long term evolution of the continetents., *in* Brown, M., and Rushmer, T., eds., Evolution and Differentiation of the Continental Crust, Cambridge University Press, p. 67-91.
Schaefer, B. F., Pearson, D. G., Rogers, N. W., and Barnicoat, A. C., 2010, Re,ÄìOs isotope and PGE constraints on the timing and origin of gold mineralisation in the Witwatersrand Basin: Chemical Geology, v. 276, no. 1,Äì2, p. 88-94.
Schaefer, B. F., Turner, S. P., Rogers, N. W., Hawkesworth, C. J., Williams, H. M., Pearson, G. D., and Nowell, G. M., 2000, Re-Os isotope characteristics of postorogenic lavas: Implications for the nature of young lithospheric mantle and its contribution to basaltic magmas: Geology, v. 28, no. 6, p. 563-566.
Shellnutt, J. G., and Zhou, M.-F., 2007, Permian peralkaline, peraluminous and metaluminous A-typegranites in the Panxi district, SW China: Their relationship to the Emeishan mantle plume: Chemical Geology, v. 243, p. 286-316.
Shirey, S. B., and Walker, R. J., 1995, Carius tube digestion for low-blank rhenium-osmium analysis.: Analytical Chemistry, v. 67, p. 2136-2141.
-, 1998, The Re-Os isotope system in cosmochemistry and high-temperautre geochemistry: Annual Review of Earth and Planetary Sciences, v. 26, p. 423-500.
Siguigna, A. P., Larabee, A. J., and Waddington, J. C., 1982, The half life of ^{176}Lu by a γ-γ coincidence measurement: Can. J. Phys., v. 60, p. 361-364.
Stewart, J. R., and Betts, P. G., 2010a, Late Paleo-Mesoproterozoic plate margin deformation in the southern Gawler Craton: Insights from structural and aeromagnetic analysis: Precambrian Research, v. 177, no. 1,Äì2, p. 55-72.
Stewart, J. R., and Betts, P. G., 2010b, Late Paleo-Mesoproterozoic plate margin deformation in the southern Gawler Craton: Insights from structural and aeromagnetic analysis: Precambrian Research, v. 177, p. 55-72.
Stewart, K. P., 1994, High temperature felsic volcanism and the role of mantle magmas in Proterozoic Crustal growth [PhD: Adelaide University.
Stewart, K. P., and Foden, J., 2001, Mesoproterozoic granitoids of South Australia: Part 1 Ð the Gawler Craton: University of Adelaide (unpublished).
Sundberg, M., Hirth, G., and Kelemen, P. B., 2010, Trapped Melt in the Josephine Peridotite: Implications for Permeability and Melt Extraction in the Upper Mantle: Journal of Petrology, v. 51, no. 1-2, p. 185-200.

Swain, G., Barovich, K., Hand, M., Ferris, G., and Schwarz, M., 2008, Petrogenesis of the St Peter Suite, southern Australia: Arc magmatism and Proterozoic crustal growth of the South Australian Craton: Precambrian Research, v. 166, p. 283-296.

Swain, G., Woodhouse A., Hand, M., Barovich, K., Schwarz, M., and Fanning, C. M., 2005, Provenance and tectonic development of the late Archean Gawler Craton, Australia; U-Pb zircon, geochemical and Sm-Nd isotopic implications: Precambrian Research, v. 141, p. 106-136.

Turner, S., Arnaud, N., Liu, J., Rogers, N., Hawkesworth, C., Harris, N., Kelley, S., Van Calsteren, P., and Deng, W., 1996a, Post-collision, Shoshonitic Volcanism on the Tibetan Plateau: Implications for Convective Thinning of the Lithosphere and the Source of Ocean Island Basalts: Journal of Petrology, v. 37, no. 1, p. 45-71.

Turner, S., and Foden, J., 1996, Magma mingling in late-Delamerian A-type granites at Mannum, south Australia: Mineralogy and Petrology, v. 56, no. 3-4, p. 147-169.

Turner, S. P., 1996, Petrogenesis of the late-Delamerian gabbroic complex at Black Hill, South Australia: Implications for convective thinning of the lithospheric mantle: Mineralogy and Petrology, v. 56, no. 1, p. 51-89.

Turner, S. P., and Foden, J., 1990, The nature of mafic magmatism through the development of the Adelaide Geosyncline and the subsequent Delamerian Orogeny, South Australia., *in* Parker, A. J., Rickwood, P. C., and Tucker, D. H., eds., Mafic Dykes and Emplacement Mechanisms: Rotterdam, A. A. Balkema, p. 431-434.

Turner, S. P., Foden, J. D., and Morrison, R. S., 1992, Derivation of Some A-Type Magmas by Fractionation of Basaltic Magma - an Example from the Padthaway Ridge, South Australia: Lithos, v. 28, no. 2, p. 151-179.

Turner, S. P., Kelley, S. P., VandenBerg, A. H. M., Foden, J. D., Sandiford, M., and Flottmann, T., 1996b, Source of the Lachlan fold belt flysch linked to convective removal of the lithospheric mantle and rapid exhumation of the Delamerian-Ross fold belt: Geology, v. 24, no. 10, p. 941-944.

Turner, S. P., and Rushmer, T., 2009, Similarities between mantle-derived A-type granites and voluminous rhyolites in continental flood basalts provinces: Earth and Environmental Science Transactions of the Royal Society of Edinburgh, v. 100, p. 1-10.

Villaseca, C., Orejana, D., and Belousova, E. A., 2012, Recycled metaigneous crustal sources for S- and I-type Variscan granitoids from the Spanish Central System batholith: Constraints from Hf isotope zircon composition: Lithos, v. 153, p. 84-93.

Vissers, R. L. M., Drury, M. R., Hoogerduijn, Strating, E. H., Spiers, C. J., and van der Wal, D., 1995, Mantle shear zones and their effect on lithosphere strength during continental breakup: Tectonophysics, v. 249, no. 3,Äì4, p. 155-171.

Wade, B. P., Barovich, K. M., Hand, M., Scrimgeour, I. R., and Close, D. F., 2006, Evidence for Early Mesoproterozoic Arc Magmatism in the Musgrave Block, Central Australia: Implications for Proterozoic Crustal Growth and Tectonic Reconstructions of Australia: Journal of Geology, v. 114, no. 1, p. 43-63.

Watson, E., Wark, D., and Thomas, J., 2006, Crystallization thermometers for zircon and rutile: Contributions to Mineralogy and Petrology, v. 151, no. 4, p. 413-433.

Whalen, J. B., Currie, K. L., and Chappell, B. W., 1987, A-type granites; geochemical characteristics, discrimination and petrogenesis: Contributions to Mineralogy and Petrology, v. 95, no. 4, p. 407-419.
Widom, E., Hoernle, K. A., Shirey, S. B., and Schmincke, H.-U., 1999, Os Isotope Systematics in the Canary Islands and Madeira: Lithospheric Contamination and Mantle Plume Signatures: Journal of Petrology, v. 40, no. 2, p. 279-296.

Figure 1a

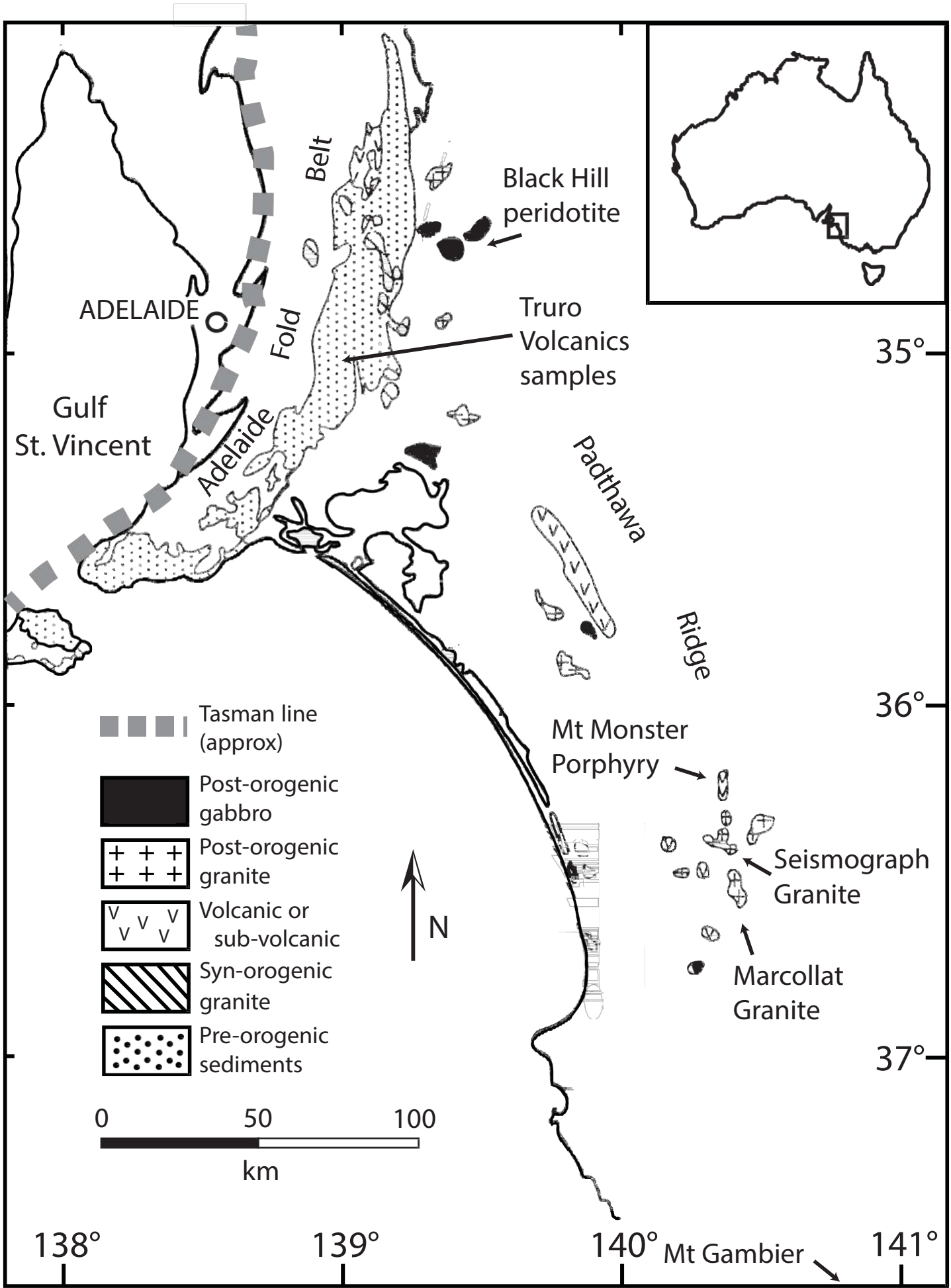
Belt
Black Hill
peridotite
ADELAIDE
Fold
Truro
Volcanics
samples
35°
Gulf
St. Vincent
Adelaide
Padthawa
Ridge
36°
Tasman line
(approx)
Mt Monster
Porphyry
Post-orogenic
gabbro
Post-orogenic
granite
Seismograph
Granite
Volcanic or
sub-volcanic
N
Syn-orogenic
granite
Marcollat
Granite
Pre-orogenic
sediments
37°
0
50
100
km
138°
139°
140°
Mt Gambier
141°

Figure 1b

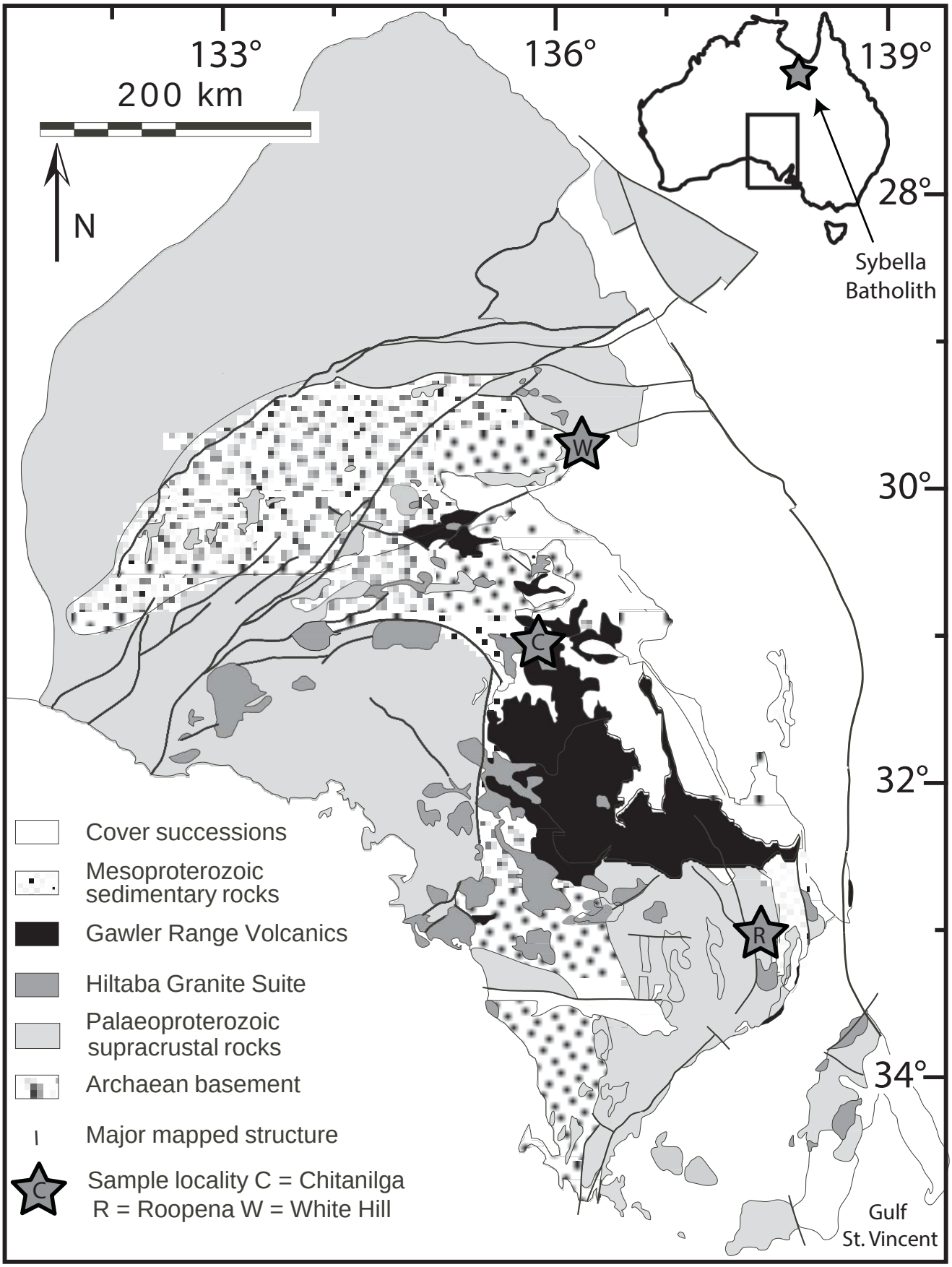
133°
136°
139°
200 km
N
28°
30°
32°
34°
Sybella
Batholith
W
C
R
Cover successions
Mesoproterozoic
sedimentary rocks
Gawler Range Volcanics
Hiltaba Granite Suite
Palaeoproterozoic
supracrustal rocks
Archaean basement
Major mapped structure
Sample locality C = Chitanilga
R = Roopena W = White Hill
Gulf
St. Vincent

Figure 3a

Figure 3a

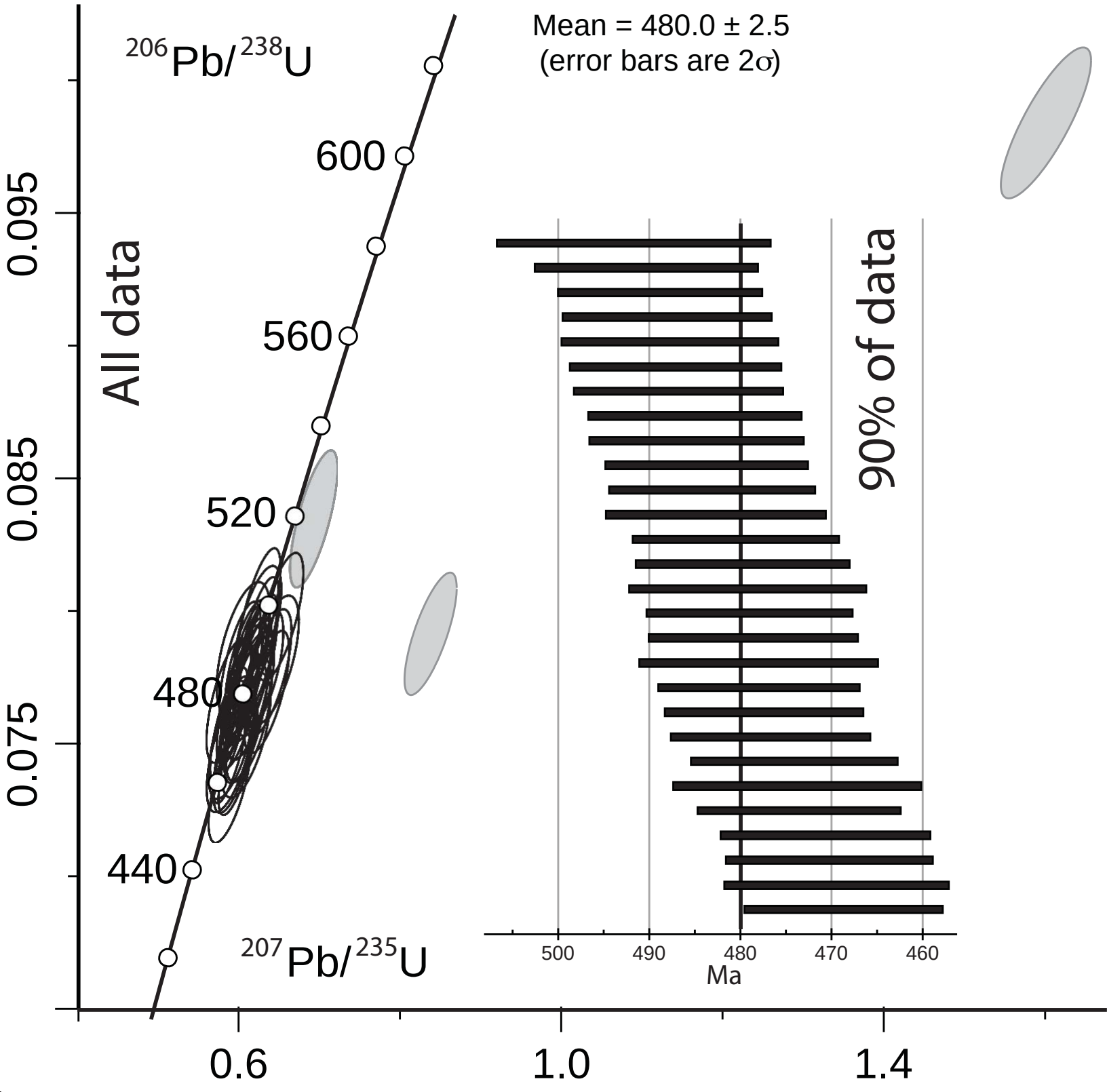

Figure 3b

Figure 3b

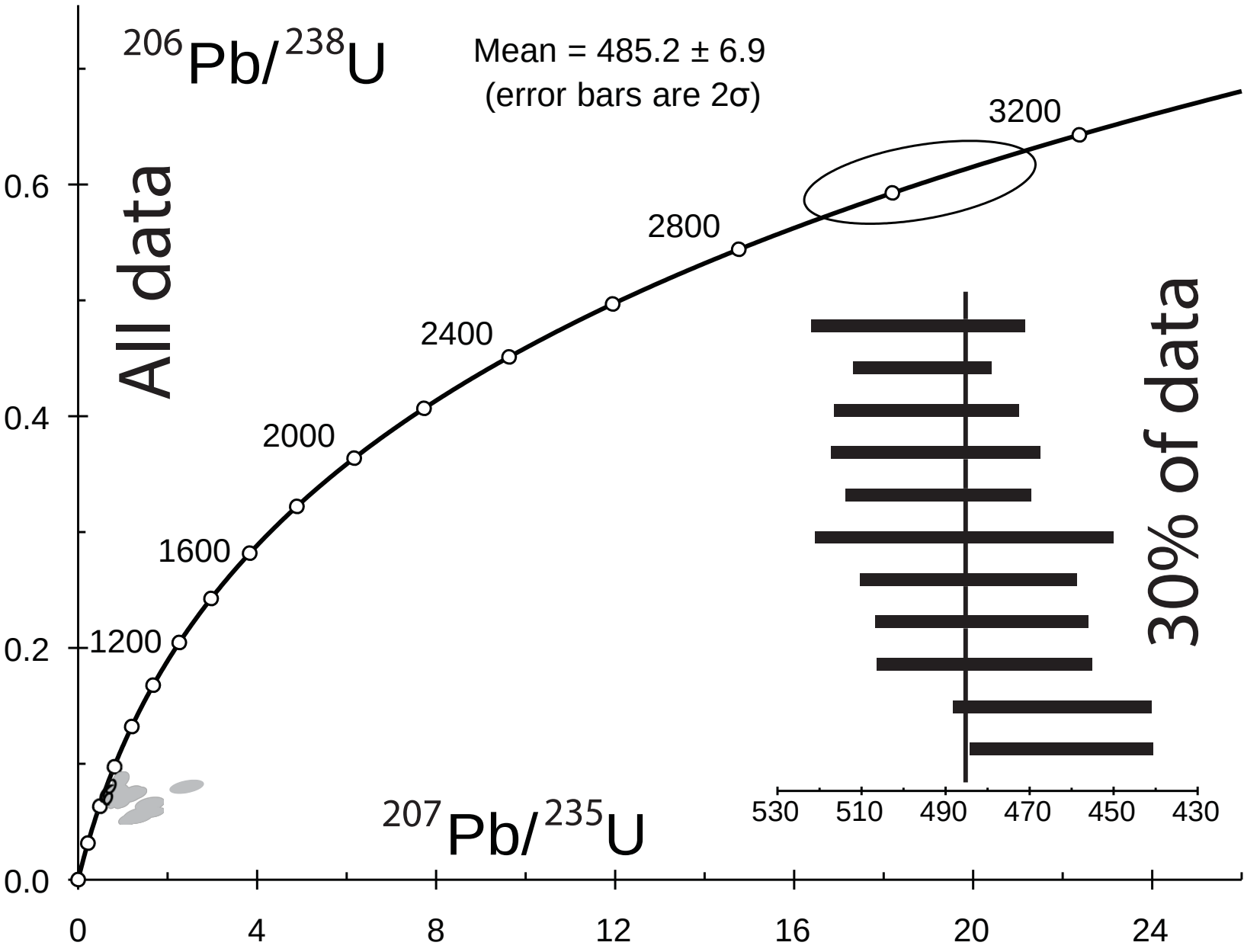

Figure 4

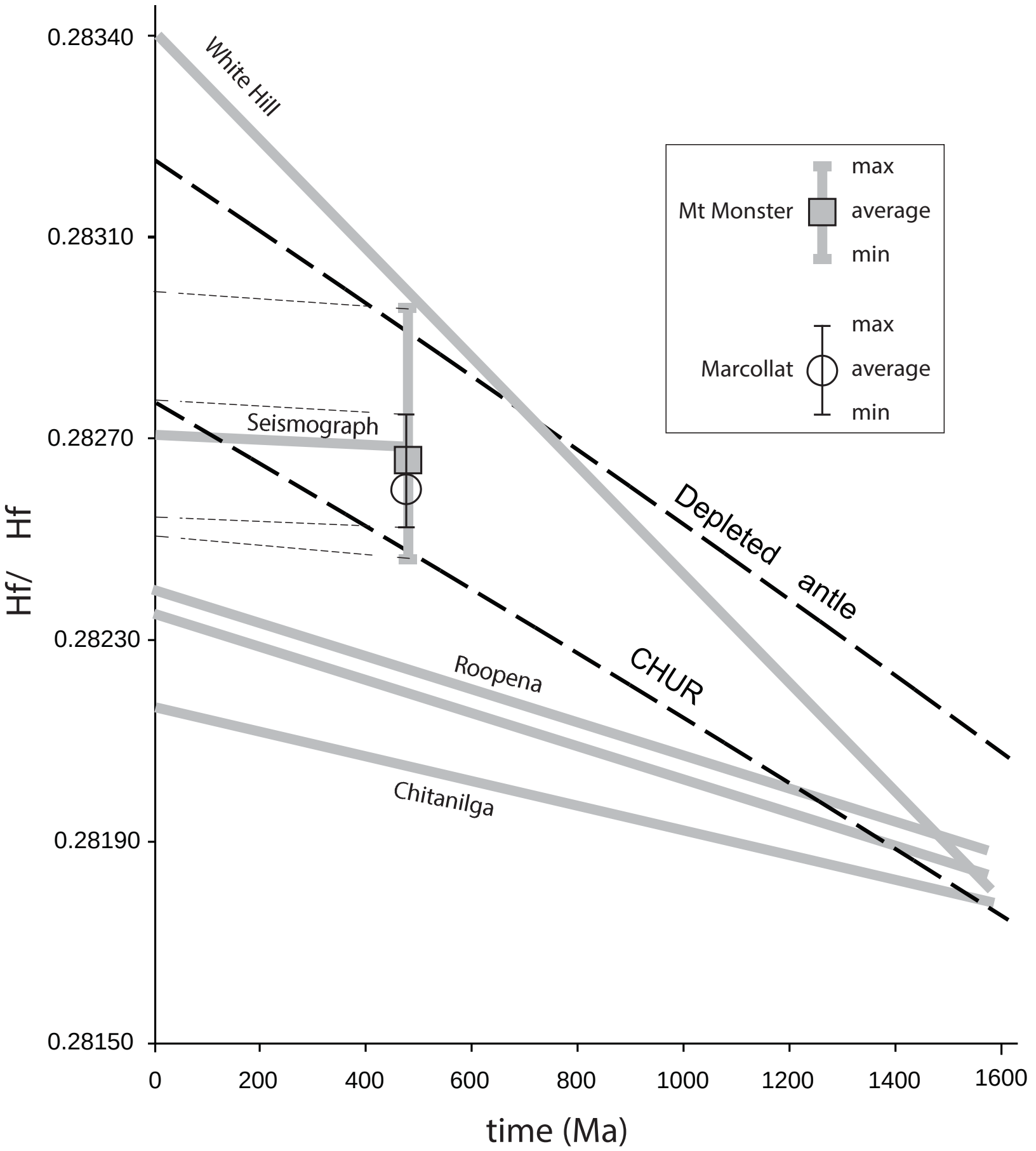
0.28340
0.28310
0.28270
0.28230
0.28190
0.28150
Hf/ Hf
0
200
400
600
800
1000
1200
1400
1600
time (Ma)
White Hill
Seismograph
Roopena
Chitanilga
Depleted antle
CHUR
Mt Monster
max
average
min
Marcollat
max
average
min

Figure 5

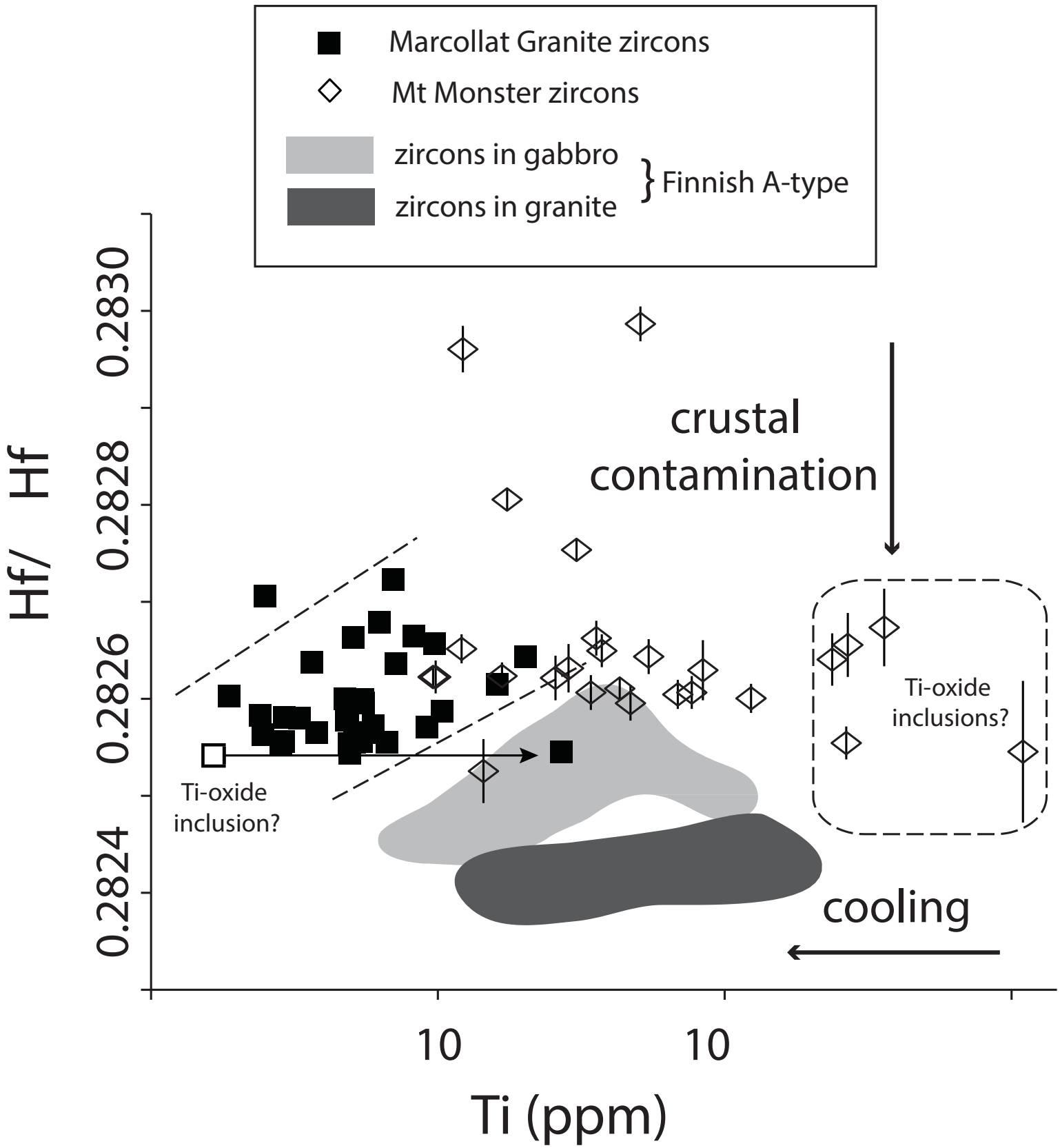
Marcollat Granite zircons
Mt Monster zircons
zircons in gabbro
zircons in granite
Finnish A-type
crustal contamination
Ti-oxide inclusions?
Ti-oxide inclusion?
cooling
Hf/ Hf
0.2824
0.2826
0.2828
0.2830
10
10
Ti (ppm)

Figure 2a

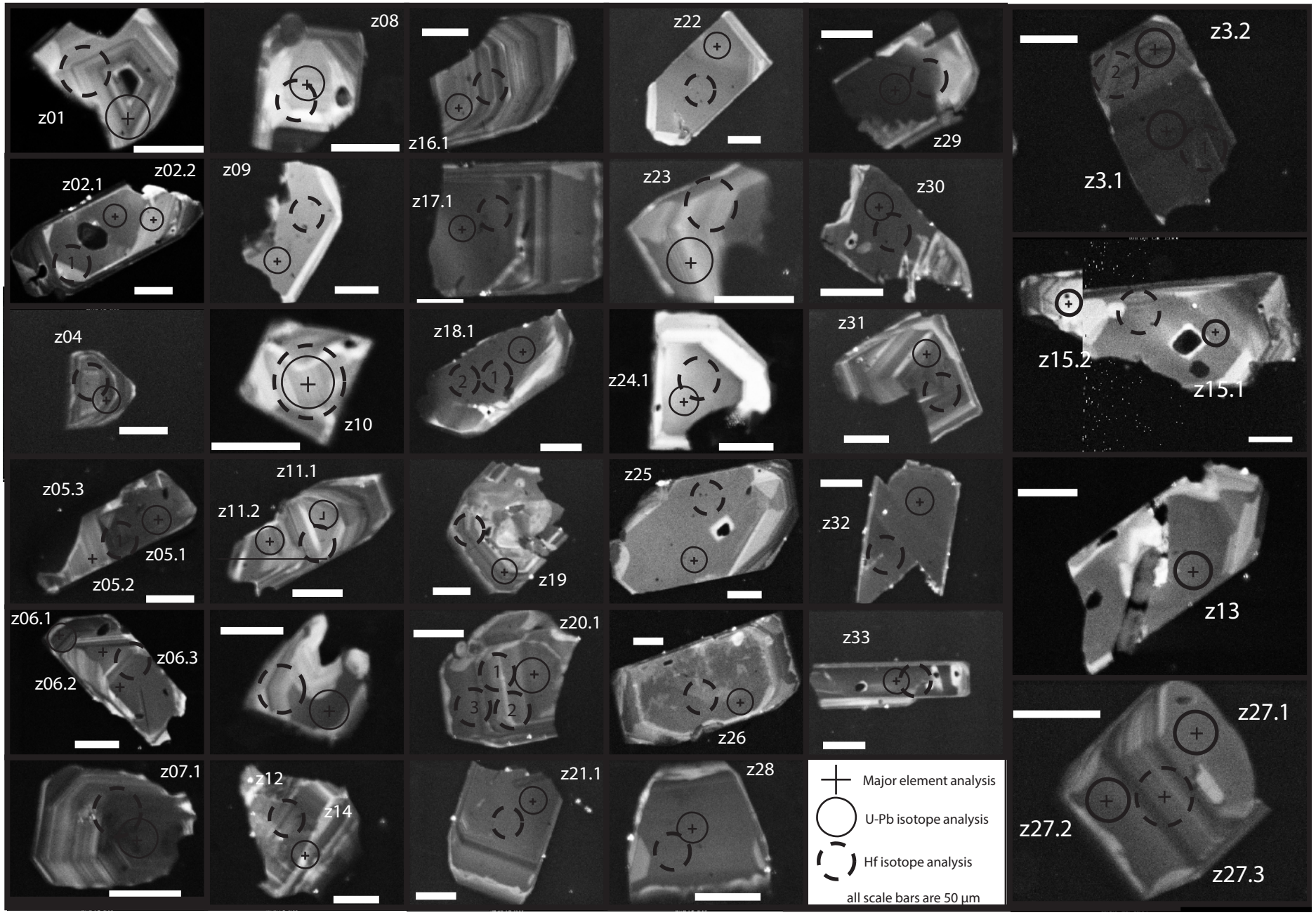
z01
z08
z16.1
z22
z29
z3.2
z3.1
z02.1
z02.2
z09
z17.1
z23
z30
z15.2
z15.1
z04
z10
z18.1
z24.1
z31
z05.3
z05.1
z05.2
z11.1
z11.2
z19
z25
z32
z13
z06.1
z06.3
z06.2
z20.1
z26
z33
z27.1
z27.2
z27.3
z07.1
z12
z14
z21.1
z28
Major element analysis
U-Pb isotope analysis
Hf isotope analysis
all scale bars are 50 µm

Figure 2b

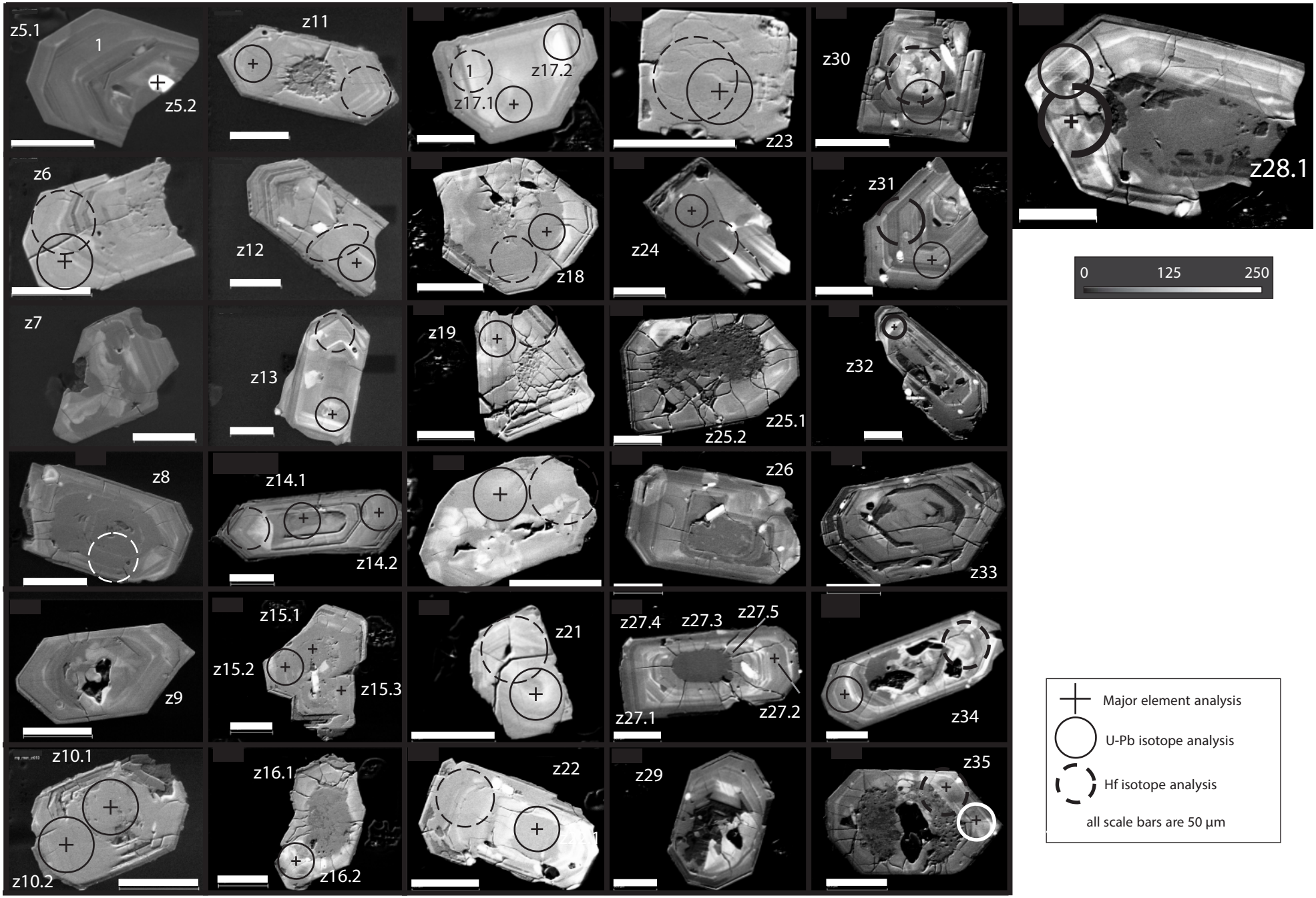

Figure 2b

Figure 6

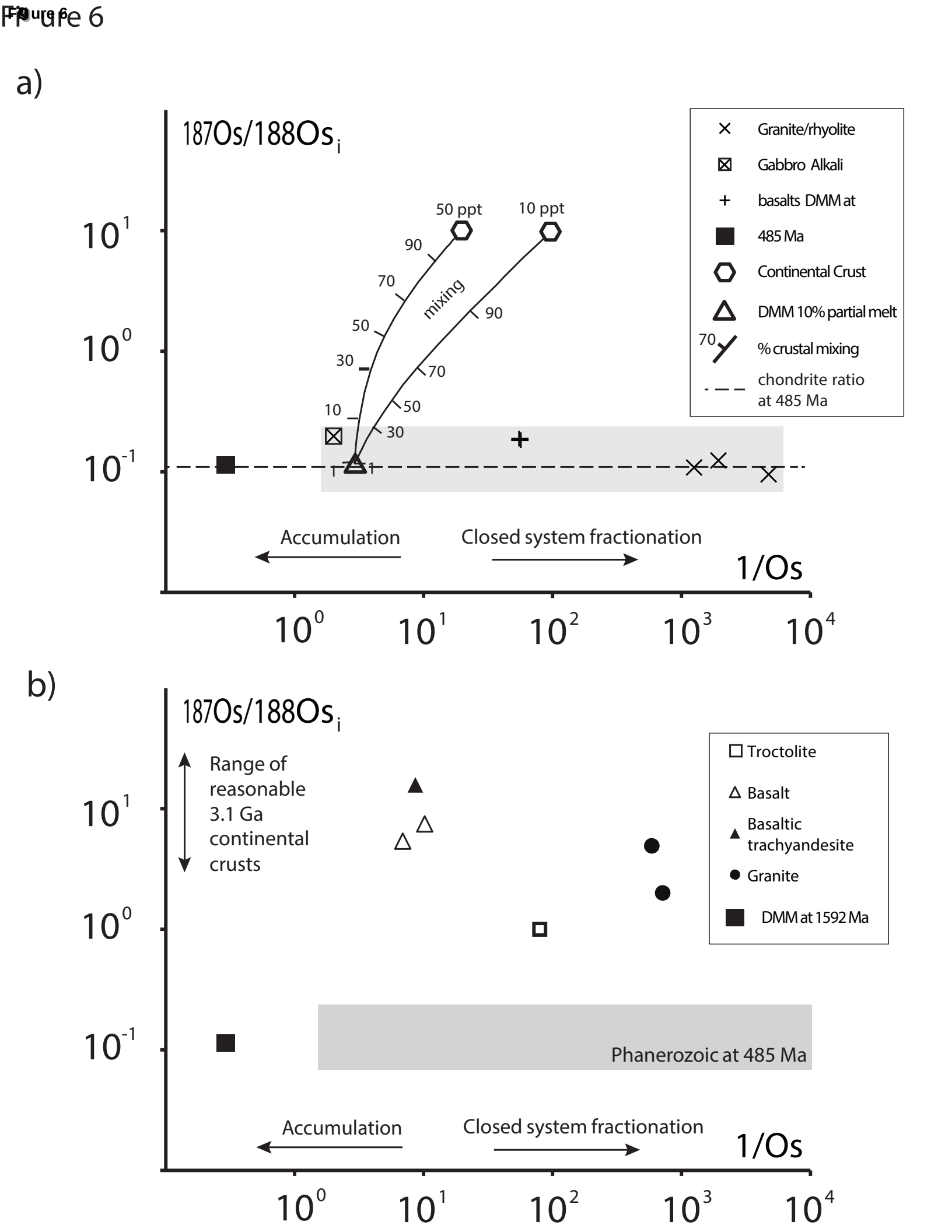
a)
$^{187}Os/^{188}Os_i$
10^1
10^0
10^{-1}
50 ppt
10 ppt
90
70
50
30
10
mixing
90
70
50
30
1
Granite/rhyolite
Gabbro Alkali
basalts DMM at
485 Ma
Continental Crust
DMM 10% partial melt
70
% crustal mixing
chondrite ratio
at 485 Ma
Accumulation
Closed system fractionation
1/Os
10^0
10^1
10^2
10^3
10^4
b)
$^{187}Os/^{188}Os_i$
Range of
reasonable
3.1 Ga
continental
crusts
Troctolite
Basalt
Basaltic
trachyandesite
Granite
DMM at 1592 Ma
Phanerozoic at 485 Ma
Accumulation
Closed system fractionation
1/Os

Table 1

In situ major, trace and isotopic data from the Marcollat Granite zircon population.

Analysis	z01	z02.1	z03.1	z03.2	z04	z05.1	z05.2	z05.3	z06.1	z06.2	z06.3	z07.1	z08	z09	z10
ZrO_2 (wt.%)	66.51	67.38	67.26	67.57	66.64	67.70	67.35	62.21	66.62	66.88	66.91	67.20	67.62	66.99	67.77
SiO_2	32.50	32.77	32.75	32.78	32.61	32.61	32.93	31.94	32.67	32.77	32.71	32.45	32.89	32.80	32.73
HfO_2	1.03	0.96	1.07	1.16	1.08	0.90	1.09	3.75	1.45	1.08	1.01	0.91	1.04	1.06	1.47
Ti[a] (ppm)	5.60	3.64	2.91	2.40	3.29	16.13			4.85			5.50	5.42	4.75	9.76
Y[a]	910.91	2118.56	2060.21	1237.84	1260.09	2070.31			1938.44			2438.62	868.98	2153.00	1539.62
Yb[a]	242.91	509.49	513.40	325.21	336.33	529.10			481.53			584.79	248.30	537.77	435.51
Hf[a]	8710.44	8135.51	9110.68	9110.68	9157.32	9281.97			8542.54			7675.05	8812.19	9024.19	12457.65
Th[a]	97.28	162.95	222.74	146.06	189.22	190.86			341.08			376.10	100.60	167.08	155.30
U[a]	140.77	179.81	399.44	247.13	279.44	313.25			361.00			350.09	140.19	180.75	205.38
$^{207}Pb/^{206}Pb$	0.0568	0.0579	0.0563	0.0561	0.0568	0.0598			0.0574			0.0764	0.0590	0.0579	0.0564
1σ	0.0012	0.0009	0.0008	0.0008	0.0009	0.0010			0.0009			0.0012	0.0011	0.0010	0.0010
$^{207}Pb/^{235}U$	0.5890	0.5986	0.5966	0.5950	0.5906	0.6923			0.6233			0.8381	0.6354	0.6080	0.6103
1σ	0.0119	0.0098	0.0087	0.0093	0.0093	0.0120			0.0101			0.0132	0.0120	0.0107	0.0113
$^{206}Pb/^{238}U$	0.0752	0.0750	0.0768	0.0770	0.0754	0.0839			0.0788			0.0795	0.0781	0.0762	0.0785
1σ	0.0009	0.0009	0.0009	0.0009	0.0009	0.0011			0.0009			0.0009	0.0010	0.0009	0.0010
$^{208}Pb/^{232}Th$	0.0246	0.0243	0.0252	0.0249	0.0244	0.0278			0.0248			0.0292	0.0252	0.0242	0.0248
1σ	0.0007	0.0006	0.0006	0.0006	0.0006	0.0009			0.0007			0.0009	0.0006	0.0006	0.0006
$^{176}Hf/^{177}Hf_m$	0.282565	0.282638	0.282581	0.282583	0.282580	0.282615		0.282610			0.282585	0.282596	0.282556	0.282600	0.282657
1σ	0.000011	0.000012	0.000009	0.000008	0.000010	0.000012		0.000009			0.000012	0.000009	0.000006	0.000007	0.000017
$^{176}Lu/^{177}Hf_m$	0.000667	0.001682	0.001826	0.001078	0.001129	0.003582		0.001871			0.001348	0.001287	0.001164	0.001589	0.003223
$^{176}Yb/^{177}Hf_m$	0.034890	0.095212	0.108550	0.063080	0.063840	0.147714		0.105373			0.074513	0.072220	0.064868	0.087574	0.111338
$^{206}Pb/^{238}U$ age (Ma)	467	466	477	478	469	519			489			493	485	474	487
1σ	6	5	5	6	5	6			6			6	6	6	6
$^{176}Hf/^{177}Hf_i^{(480\ Ma)}$	0.282559	0.282622	0.282564	0.282573	0.282569	0.282582		0.282593	0.282572			0.282584	0.282545	0.282585	0.282627
εHf	3.39	5.64	3.58	3.89	3.77	4.20		4.59	3.87			4.28	2.91	4.33	5.81
1σ	0.39	0.42	0.32	0.29	0.33	0.42		0.33	0.42			0.30	0.22	0.26	0.60

Major elements expressed in wt% oxides were analysed by EMP with a 15 kV accelerating voltage and 20 nA beam.
EMP standards used had the following composition; Hf: Hf wire (Hf, 100%); Zr, O: zircon (O, 34.78%; Si, 15.26%; P, 0.04%; Y, 0.05%; Zr, 48.97%; Hf, 0.9%); and Y: YAG (Y, 44.93%; O, 32.34%; Al, 22.73%). Pb, Th and U isotopes were measured by quadropole ICPMS. Each mass had a dwell time of 10 ms except ^{238}U and ^{206}Pb (15 ms) and ^{207}Pb (30 ms).
Hf, Lu and Yb isotope ratios were measured by multicollector ICPMS. bd = below detection limit.
A ^{176}Lu decay constant of 1.93×10^{-11} (Blichert-Toft and Albarède, 1997) was used to calculate initial $^{176}Hf/^{177}Hf$ ratios.
A CHUR$_{t=0}$ value of 0.282772 and $^{176}Lu/^{177}Hf$ ratio of 0.0332 (Blichert-Toft and Albarède, 1997) was used to calculate εHf.
Hf isotope ratios with no direct corresponding major element analysis were corrected using the data from within the same grain.
[a]Data from the same spots analysed, see Pankhurst (2012).

Table 1 (continued)

Analysis	z11.1	z11.2	z12	z13	z14	z15.1	z15.2	z16.1	z17.1	z18.1	z18.2	z19	z20.1	z20.2	z20.3	z21.1
ZrO_2 (wt.%)	68.03	68.07	66.77	66.93	67.64	66.97	67.94	67.37	67.37	67.09		67.31	67.62			66.85
SiO_2	32.92	32.82	32.67	32.65	32.60	32.62	32.84	32.62	32.63	32.73		32.49	32.69			32.71
HfO_2	1.03	0.90	1.43	0.89	1.51	0.99	1.47	1.15	1.20	1.06		1.86	1.16			1.25
Ti[a] (ppm)	5.95	5.37	4.92	4.80	6.25	8.26	6.91	2.90	6.66	2.49		10.34	6.99			5.47
Y[a]	1538.43	962.64	1007.52	1068.86	1694.32	1197.27	1296.31	1613.67	1024.57	2602.57		2510.65	2149.02			1230.94
Yb[a]	350.39	254.80	289.30	281.35	462.13	320.04	359.63	421.65	280.87	634.21		675.08	544.76			337.61
Hf[a]	7591.95	8698.57	12141.36	7505.46	12844.33	8400.92	12447.48	9742.43	10213.05	8957.20		15788.51	9818.74			10570.90
Th[a]	152.69	112.91	91.44	127.56	251.08	143.59	94.15	151.66	108.23	208.56		337.33	267.45			127.36
U[a]	160.20	155.54	168.24	164.11	367.44	172.47	127.40	253.17	156.85	261.61		528.16	416.39			175.46
$^{207}Pb/^{206}Pb$	0.0595	0.0576	0.0580	0.0573	0.0568	0.0553	0.0555	0.0572	0.0576	0.0570		0.0568	0.1176			0.0578
1σ	0.0011	0.0010	0.0011	0.0010	0.0009	0.0011	0.0012	0.0010	0.0011	0.0009		0.0009	0.0016			0.0011
$^{207}Pb/^{235}U$	0.6343	0.6119	0.6248	0.6198	0.6098	0.5871	0.6051	0.6198	0.6136	0.6240		0.6014	1.6011			0.5886
1σ	0.0112	0.0110	0.0122	0.0111	0.0098	0.0112	0.0134	0.0109	0.0121	0.0102		0.0096	0.0228			0.0107
$^{206}Pb/^{238}U$	0.0774	0.0771	0.0781	0.0784	0.0779	0.0771	0.0790	0.0786	0.0773	0.0794		0.0767	0.0988			0.0739
1σ	0.0009	0.0009	0.0010	0.0010	0.0009	0.0010	0.0010	0.0010	0.0010	0.0009		0.0009	0.0012			0.0009
$^{208}Pb/^{232}Th$	0.0249	0.0241	0.0255	0.0242	0.0240	0.0241	0.0254	0.0240	0.0246	0.0250		0.0241	0.0875			0.0229
1σ	0.0006	0.0006	0.0007	0.0007	0.0007	0.0007	0.0008	0.0008	0.0008	0.0006		0.0006	0.0023			0.0007
$^{176}Hf/^{177}Hf_m$	0.282572		0.282544	0.282578	0.282679	0.282665		0.282556	0.282555	0.282706	0.282776	0.282587	0.282723	0.282638	0.282576	0.282599
1σ	0.000008		0.000010	0.000012	0.000009	0.000012		0.000010	0.000011	0.000014	0.000014	0.000009	0.000015	0.000008	0.000009	0.000009
$^{176}Lu/^{177}Hf_m$	0.001161		0.000608	0.000865	0.001571	0.001677		0.001008	0.000748	0.002064	0.002008	0.000852	0.001345	0.000991	0.001010	0.000781
$^{176}Yb/^{177}Hf_m$	0.063857		0.033852	0.047294	0.093548	0.095373		0.059210	0.041535	0.119998	0.123863	0.052390	0.084752	0.061841	0.060226	0.046954
$^{206}Pb/^{238}U$ age (Ma)	480	479	485	487	484	479	490	488	480	493		477	607			460
1σ	6	6	6	6	6	6	6	6	6	6		5	7			5
$^{176}Hf/^{177}Hf_i^{(480\ Ma)}$	0.282561		0.282538	0.282570	0.282664	0.282649		0.282547	0.282548	0.282687	0.282757	0.282579	0.282710	0.282629	0.282567	0.282592
εHf	3.48		2.67	3.79	7.13	6.60		2.96	3.01	7.92	10.42	4.11	8.76	5.87	3.67	4.56
1σ	0.28		0.35	0.42	0.30	0.42		0.35	0.39	0.49	0.49	0.31	0.53	0.29	0.33	0.31

Table 1 (continued)

Analysis	z22	z23	z24.1	z25	z26	z27.1	z27.2	z27.3	z28	z29	z30	z31	z32	z33
ZrO_2 (wt.%)	67.33	67.28	67.94	67.11	67.16	67.09	67.07	66.74	67.87	67.34	66.40	67.22	66.61	67.11
SiO_2	32.74	32.61	32.77	32.74	32.84	32.86	32.77	32.61	32.31	32.64	32.57	32.71	32.64	32.73
HfO_2	1.02	1.06	0.91	1.03	1.05	1.23	1.11	1.48	1.23	1.12	1.14	1.07	1.25	1.08
Ti[a] (ppm)	7.15	3.77	5.12	5.06	21413.19	4.90	4.01		2.45	9.14	2.84	1.87	20.19	26.94
Y[a]	1207.98	1264.00	909.79	1952.85	1048.84	1036.24	1555.97		1103.91	4683.60	2776.13	468.44	4727.19	1594.32
Yb[a]	327.51	333.88	236.28	485.68	298.13	297.54	444.05		317.80	1096.71	691.73	142.79	1125.63	434.97
Hf[a]	8621.40	9014.86	7746.28	8722.31	8885.97	10430.14	12565.35		10390.28	9503.30	9634.74	9077.61	10564.97	9191.24
Th[a]	145.26	163.74	103.38	158.81	86.03	133.08	190.52		130.90	589.28	363.28	55.56	799.19	161.86
U[a]	170.25	243.02	128.75	178.36	146.39	172.81	358.72		285.68	408.29	576.50	130.50	1276.19	193.76
$^{207}Pb/^{206}Pb$	0.0582	0.0573	0.0583	0.0566	0.0592	0.0567	0.0560		0.0564	0.0556	0.0563	0.0574	0.0564	0.0588
1σ	0.0011	0.0010	0.0012	0.0011	0.0012	0.0011	0.0009		0.0010	0.0009	0.0009	0.0010	0.0010	0.0011
$^{207}Pb/^{235}U$	0.6120	0.6145	0.6086	0.5909	0.6414	0.6228	0.5876		0.6030	0.6011	0.6085	0.5944	0.6242	0.6507
1σ	0.0115	0.0107	0.0124	0.0117	0.0132	0.0120	0.0096		0.0102	0.0103	0.0095	0.0107	0.0110	0.0117
$^{206}Pb/^{238}U$	0.0763	0.0778	0.0757	0.0757	0.0786	0.0797	0.0761		0.0776	0.0785	0.0784	0.0751	0.0803	0.0802
1σ	0.0009	0.0009	0.0010	0.0009	0.0010	0.0010	0.0009		0.0009	0.0009	0.0009	0.0009	0.0010	0.0010
$^{208}Pb/^{232}Th$	0.0236	0.0243	0.0240	0.0238	0.0254	0.0260	0.0240		0.0252	0.0253	0.0251	0.0237	0.0257	0.0251
1σ	0.0007	0.0008	0.0008	0.0008	0.0009	0.0007	0.0007		0.0008	0.0007	0.0008	0.0008	0.0010	0.0009
$^{176}Hf/^{177}Hf_m$	0.282636	0.282565	0.282555	0.282663	0.282566			0.282554	0.282563	0.282571	0.282552	0.282603	0.282643	0.282545
1σ	0.000010	0.000010	0.000008	0.000011	0.000010			0.000008	0.000007	0.000010	0.000009	0.000009	0.000008	0.000026
$^{176}Lu/^{177}Hf_m$	0.001964	0.000779	0.001083	0.001643	0.001976			0.000950	0.000910	0.001384	0.001644	0.001400	0.003067	0.002063
$^{176}Yb/^{177}Hf_m$	0.114020	0.043178	0.059067	0.091227	0.110493			0.048968	0.047125	0.072097	0.090061	0.079231	0.184937	0.101426
$^{206}Pb/^{238}U$ age (Ma)	474	483	471	470	488	492	469		479	478	483	474	493	509
1σ	6	6	6	6	6	8	6		6	7	6	7	7	7
$^{176}Hf/^{177}Hf_i^{(480\ Ma)}$	0.282618	0.282558	0.282545	0.282648	0.282548			0.282545	0.282555	0.282558	0.282537	0.282590	0.282614	0.282526
εHf	5.48	3.35	2.90	6.54	3.00			2.91	3.24	3.37	2.61	4.49	5.36	2.22
1σ	0.34	0.34	0.27	0.39	0.34			0.28	0.25	0.35	0.32	0.33	0.29	0.91

Table 2

In situ major, trace and isotopic data from the Mt Monster Porphyry zircon population.

Analysis	monzr5.1	monzr6.1	monzr7.1	monzr8.1	monzr9.1	monzr10.1	monzr10.2	monzr11.1	monzr12.1	monzr13.1	monzr14.1	monzr14.2	monzr15.1	monzr15.2	monzr16.1
ZrO_2(wt.%)	63.14	64.85	65.22	63.42	64.57	59.55	63.72	64.49	64.28	64.73	63.92	64.41	63.06	63.98	61.17
SiO_2	31.09	31.87	32.03	31.82	31.96	30.52	31.66	31.70	31.86	31.59	31.31	31.19	31.63	31.82	31.03
HfO_2	1.42	1.52	1.25	1.84	1.66	1.40	1.65	1.46	1.08	1.10	1.20	1.47	1.78	1.73	1.83
Y_2O_3	0.70	0.31	0.19	0.62	0.15	2.67	0.52	0.21	0.84	0.30	0.55	0.18	0.69	0.40	1.47
P (ppm)	391.66	488.11	575.37	494.17	450.2	1146.22	408.61	834.89	457.49	789.96	421.11	428.93		681.57	
Ti	30.32	12.12	17.33	50.79	14.31	22.11	36.11	42.97	363.28	9.73	34.05	10.64		110.33	
Y	2818.55	2087.36	691.33	6210.86	2052.16	5067.97	3801.04	2279.63	5674.21	2989.23	13433.08	6941.82		7547.79	
Nb	23.91	15.97	9.6	43.25	12.42	26.45	52.42	21.14	15.13	11.86	39.23	23.95		134.62	
La	9.85	8.55	6.38	27.2	46.26	21.47	7.19	164.61	50.16	167.53	166.26	34.23		19.86	
Ce	117.68	68.94	47.54	388.17	277.4	111.37	105.94	380.87	483.41	243.05	1605.89	698.82		348.75	
Pr	6.75	3.47	2.6	17.8	13.05	9.44	4.06	32.39	14.3	31.06	59.77	29.54		9.33	
Nd	35.38	15	11.56	91.19	49.98	50.7	23.07	125.97	68.12	125.06	258.55	140.2		43.39	
Sm	19.68	9.71	7.14	54.13	22.63	27.11	16.57	27.19	42.97	34.06	138.42	81.97		27.99	
Eu	1.06	0.48	0.317	2.59	1.14	0.8	0.68	1.08	2.74	2.63	10.04	4.59		1.08	
Gd	55.19	38.54	14.57	135.56	41.82	80.32	63.76	49.92	145.4	76.63	312.36	157.95		115.86	
Tb	22.03	14.47	5.2	47.9	16.32	33.08	24.18	17.93	51.29	23.72	110.33	58.5		41.97	
Dy	265.47	179.15	61.41	555.36	179.51	432.28	318.35	196.93	579.18	266.55	1165.2	622.9		561.93	
Ho	91.88	69.54	21.72	193.07	64.91	169.43	122.98	71.37	199.35	98.98	369.77	211.12		220.56	
Er	413.73	320.46	101.73	803.24	295.77	785.09	583.6	323.64	842.5	418.73	1474.94	869.77		1044.83	
Tm	89.95	69.94	22.95	165.88	66	170.17	133.66	69.07	170.05	81.18	288.83	175.11		224.36	
Yb	858.4	670.09	219.12	1501.31	684.77	1723.93	1322.48	644.83	1521.56	730.56	2417.95	1561.59		2070.54	
Lu	143.74	116.85	41.23	234.72	115.1	299.38	223.23	114.61	257.05	128.52	346.79	239.33		352.25	
Hf	12042.99	12912.17	10592.95	15627.4	14114.6	11900.53	13951.79	12398.3	9126.79	9348.96	10158.78	12455.96		14653.92	
Ta	4.5	4.14	2.21	11.45	9.19	7.35	16.58	4.55	2	2.27	8.62	8.84		37.08	
Pb	28.8	30.18	11.48	53.3	19.04	107.69	72.35	47.43	89.37	24.83	67.73	44.22		168.61	
Th	509.34	637.99	107.64	1044.21	406.5	2016.36	1347.41	713.55	876.38	452.6	1124.7	664.48		3451.88	
U	917.12	1066.84	269.27	2146.79	1123.71	3064.94	2843.25	1075.79	851.39	679.41	1113.98	1293.27		5834.43	
$^{207}Pb/^{206}Pb$	0.0461	0.0636	0.0461	0.0461	0.0504	0.0697	0.0713	0.0477	0.0461	0.0620	0.1389	0.0625		0.0727	0.1915
1σ	0.0066	0.0038	0.0087	0.0048	0.0035	0.0046	0.0049	0.0145	0.0209	0.0039	0.0120	0.0042		0.0056	0.0097
$^{207}Pb/^{235}U$	0.4581	0.7058	0.4272	0.4304	0.5381	0.8775	0.8142	0.4713	0.4603	0.6361	1.0852	0.6906		0.9033	1.6561
1σ	0.0645	0.0401	0.0798	0.0440	0.0361	0.0549	0.0532	0.1421	0.2081	0.0386	0.0878	0.0447		0.0677	0.0790
$^{206}Pb/^{238}U$	0.0722	0.0806	0.0673	0.0678	0.0775	0.0914	0.0828	0.0716	0.0725	0.0744	0.0567	0.0802		0.0902	0.0628
1σ	0.0015	0.0020	0.0020	0.0017	0.0021	0.0023	0.0023	0.0020	0.0029	0.0018	0.0019	0.0021		0.0027	0.0014
$^{208}Pb/^{232}Th$	0.0231	0.0380	0.0233	0.0262	0.0284	0.0347	0.0349	0.0227	0.0273	0.0262	0.0163	0.0284		0.0313	0.0244
1σ	0.0021	0.0059	0.0045	0.0044	0.0051	0.0061	0.0066	0.0032	0.0061	0.0038	0.0035	0.0045		0.0058	0.0034
$^{176}Hf/^{177}Hf_m$	0.282753	0.282960	0.282805	0.282986	0.282525			0.282610	0.282673	0.282622	0.282606				0.282584
1σ	0.000011	0.000024	0.000012	0.000018	0.000033			0.000012	0.000040	0.000017	0.000018				0.000013
$^{176}Lu/^{177}Hf_m$	0.002193	0.004653	0.001665	0.003142	0.006677			0.002794	0.005446	0.002150	0.001002				0.003413
$^{176}Yb/^{177}Hf_m$	0.074749	0.167258	0.057288	0.137790	0.231365			0.096793	0.252503	0.075609	0.039372				0.150460
$^{206}Pb/^{238}U$ age (Ma)	449	499	420	423	481	564	513	446	451	462	356	497		557	393
1σ	9	12	12	10	13	14	13	12	17	11	12	12		16	8
$^{176}Hf/^{177}Hf_{i\,(485\ Ma)}$	0.282732	0.282916	0.282789	0.282956	0.282462			0.282584	0.282622	0.282602	0.282597				0.282552
εHf	9.65	16.16	11.67	17.58	0.09			4.39	5.74	5.03	4.84				3.26
1σ	0.39	0.84	0.42	0.63	1.16			0.42	1.40	0.60	0.63				0.46

Pb isotope ratios are common Pb corrected. Major elements expressed in wt.% oxides were analysed by EMP with a 15 kV accelerating voltage and 20 nA beam. EMP standards used had the following composition; Hf: Hf wire (Hf, 100%); Zr, O: zircon (O, 34.78%; Si, 15.26%; P, 0.04%; Y, 0.05%; Zr, 48.97%; Hf, 0.9%); and Y: YAG (Y, 44.93%; O, 32.34%; Al, 22.73%).

Concentrations calculated by quadropole ICPMS on measured isotopes as follows; ^{31}P, ^{49}Ti, ^{89}Y, ^{93}Nb, ^{139}La, ^{140}Ce, ^{141}Pr, ^{146}Nd, ^{147}Sm, ^{151}Eu, ^{157}Gd, ^{159}Tb, ^{163}Dy, ^{165}Ho, ^{166}Er, ^{169}Tm, ^{173}Yb, ^{175}Lu, ^{178}Hf, ^{181}Ta, ^{208}Pb, ^{232}Th and ^{238}U. Each mass had a dwell time of 10 ms except ^{238}U and ^{206}Pb (15 ms) and ^{207}Pb (30 ms).

Hf, Lu and Yb isotope ratios were measured by multicollector ICPMS.

A ^{176}Lu decay constant of 1.93×10^{-11} (Blichert-Toft and Albarède, 1997) was used to calculate initial $^{176}Hf/^{177}Hf$ ratios.

A $CHUR_{t=0}$ value of 0.282772 and $^{176}Lu/^{177}Hf$ ratio of 0.0332 (Blichert-Toft and Albarède, 1997) was used to calculate εHf.

Table 2 (continued)

Analysis	monzr16.2	monzr17.1	monzr17.2	monzr18.1	monzr19.1	monzr20.1	monzr21.1	monzr22.1	monzr23.1	monzr24.1	monzr25.1	monzr25.2	monzr26.1	monzr27.1	monzr27.1	monzr27.1
ZrO_2 (wt.%)	62.53	64.82	64.77	62.93	64.01	63.14	63.96	62.59	62.40	63.11	62.00	64.85	61.16	63.16	60.66	60.34
SiO_2	31.12	30.52	32.09	30.99	30.93	31.39	31.26	30.75	30.94	30.46	31.96	30.90	30.15	30.60	29.86	29.94
HfO_2	1.53	1.20	1.52	1.74	1.71	3.12	1.61	1.12	1.58	1.10	1.72	1.40	1.01	1.87	1.81	1.76
Y_2O_3	0.27	0.34	0.25	0.91	0.40	0.19	0.41	1.44	0.96	1.16	0.99	0.20	2.07	0.77	1.94	1.85
P (ppm)	7198.93	438.99	353.7	573.81	361.88	202.11	346.27	553.41	1314.43	574.62	232.58		786.91	1670.52		412.46
Ti	287.15	11.99	14.1	76.85	231.35	28.44	35.58	16.62	238.74	54.29	267.42		25.59	15.09		6.24
Y	12919.22	3080.3	1680.24	4189.85	5503.85	2563.22	2063.13	4146.13	9941.12	5919.92	1687.95		9567.09	13663.27		2272.54
Nb	56.08	6.9	5.24	53.78	80.63	66	31.67	36.23	85.68	23.44	26.29		66.16	86.51		14.97
La	72.77	0.802	0.774	15.14	18.54	9.54	3.01	20.37	61.96	4.94	3.42		18.08	1.7		3.33
Ce	1842.44	37	19.55	87.28	371.18	106	47.26	290.88	448.62	87.67	98.14		295.42	74.93		74.56
Pr	39.83	0.746	0.367	4.6	13.12	5.43	1.88	14.23	22.38	3.33	1.76		9.31	1.4		1.45
Nd	214.98	7.4	3.84	23.05	67.37	21.48	8.94	68.46	99.81	23.46	11.44		57.36	12.15		9.27
Sm	133.66	13.36	6.43	14.31	49.99	12.82	7.57	38.39	63.93	32.67	8.44		64.69	29.04		9.59
Eu	8.67	1.5	0.649	0.426	2.54	1	0.48	1.46	2.63	3.99	0.72		3.09	0.5		0.499
Gd	307.04	66.11	32.66	61.37	126.39	32.47	32.59	88.25	192.19	153.9	30.87		244.76	176.71		38.71
Tb	109.34	25.69	12.14	24.7	42.31	13.31	11.51	32.56	71.38	51.92	13.41		90.36	79.01		14.77
Dy	1188.82	289.69	153	325.78	489.42	168	158.68	376.17	843.87	586.89	148.12		1012.91	1069.96		182.8
Ho	380.94	108.7	58.92	136.19	174.19	62.39	66.66	132	314.27	209.9	57.55		356.13	450.14		72.73
Er	1530.84	466.58	260.98	660.19	755.17	299.74	331.4	600.75	1446.79	880.3	253.01		1447.31	2174.86		349.58
Tm	310.29	94.07	53.6	150.71	160.67	81.36	78.57	125.66	303.73	170.19	58.75		276.81	495.86		77.2
Yb	2962.93	868.8	497.88	1460.3	1545.97	955.31	788.47	1148.63	2811.93	1505.29	584.59		2451.35	4895.93		751.85
Lu	423.16	153.89	91.99	262.94	254.62	185.22	139.32	201.41	490.92	261.5	96.65		389.29	845.65		134.83
Hf	15519.71	10163.87	10163.87	14748.05	14512.31	26462.87	13655.85	9508.38	13437.92	9300.63	14608.98		8575.6	15836.84		13536.28
Ta	11.91	1.99	1.538	18.77	13.4	218	9.28	5.07	16.94	3.51	5.58		10.91	28.6		5.11
Pb	91.81	28.4	20.65	118.37	57.44	11.4	26.87	47.8	192.88	57.29	16.55		200.05	270.56		36.65
Th	1917.67	557.32	376.87	2139.3	1066.62	138.09	674.94	885.55	3821.98	1131.7	353.21		4042.98	6476.62		714.01
U	1648.38	627.9	475.25	4173.12	2262.44	2656.37	1521.76	1232.45	5349.61	1002.46	747.42		2763.75	13851.59		1251.86
$^{207}Pb/^{206}Pb$		0.0671	0.0618	0.0605	0.0461	0.0608	0.0556	0.0536	0.0728	0.0595	0.0717		0.0711	0.0560		0.0583
1σ		0.0024	0.0035	0.0026	0.0192	0.0033	0.0035	0.0116	0.0045	0.0040	0.0066		0.0051	0.0040		0.0041
$^{207}Pb/^{235}U$		0.7359	0.6791	0.6657	0.4264	0.6640	0.6082	0.5674	0.7856	0.6134	0.7640		0.8116	0.6182		0.6821
1σ		0.0249	0.0369	0.0270	0.1763	0.0350	0.0371	0.1217	0.0466	0.0386	0.0662		0.0548	0.0414		0.0457
$^{206}Pb/^{238}U$		0.0795	0.0797	0.0799	0.0672	0.0793	0.0794	0.0768	0.0783	0.0747	0.0776		0.0827	0.0801		0.0849
1σ		0.0013	0.0018	0.0014	0.0031	0.0019	0.0021	0.0018	0.0019	0.0020	0.0028		0.0022	0.0021		0.0022
$^{208}Pb/^{232}Th$		0.0258	0.0269	0.0268	0.0458	0.0499	0.0263	0.0240	0.0231	0.0262	0.0329		0.0354	0.0316		0.0361
1σ		0.0020	0.0033	0.0031	0.0222	0.0080	0.0049	0.0016	0.0041	0.0051	0.0088		0.0070	0.0070		0.0074
$^{176}Hf/^{177}Hf_m$		0.282651		0.282606		0.282631	0.282662	0.282623	0.282640	0.282643	0.282554		0.282621			
1σ		0.000015		0.000017		0.000025	0.000018	0.000014	0.000027	0.000018	0.000017		0.000023			
$^{176}Lu/^{177}Hf_m$		0.001850		0.002267		0.002896	0.002685	0.001984	0.004544	0.001991	0.002299		0.002943			
$^{176}Yb/^{177}Hf_m$		0.065366		0.094357		0.088906	0.102672	0.082077	0.149879	0.078271	0.081486		0.100981			
$^{206}Pb/^{238}U$ age (Ma)		493	495	495	419	492	492	477	486	465	482		512	496		525
1σ		8	11	8	19	11	12	11	11	12	17		13	13		13
$^{176}Hf/^{177}Hf_{i\ (485\ Ma)}$		0.282634		0.282585		0.282604	0.282637	0.282604	0.282597	0.282624	0.282532		0.282593			
εHf		6.15		4.42		5.10	6.27	5.12	4.87	5.82	2.57		4.73			
1σ		0.53		0.60		0.88	0.63	0.49	0.95	0.63	0.60		0.81			

Table 2 (continued)

Analysis	monzr27.4	monzr27.5	monzr28.1	monzr28.2	monzr29.1	monzr30.1	monzr31.1	monzr31.2	monzr32.1	monzr33.1	monzr34.1	monzr35			
ZrO_2 (wt.%)	63.49	64.67	64.03	62.76	63.94	64.01	62.76		64.28	63.67	64.63	63.24			
SiO_2	30.88	30.87	30.87	31.10	30.16	30.86	30.36		30.67	31.55	31.79	30.27			
HfO_2	1.60	1.39	1.35	1.82	1.42	1.47	1.44		1.58	1.01	1.45	1.23			
Y_2O_3	0.51	0.25	0.44	0.62	0.42	0.39	0.46		0.29	1.05	0.23	1.25			
P (ppm)			192.16	590.7	288.87	773.26	598.49		388.35	446.32	310.96	565.21	47.49	52.18	47.57
Ti			33.87	46.86	84.1	68.65	37.18		270.87	1113.21	9.53	124.01	12.43	23.93	11.47
Y			581.5	2097.13	2991.78	4227.69	3253.09		6381.11	9036.57	1897.11	4294	3.68	3.73	3.67
Nb			3.89	23.08	16.02	44.94	29.94		40.13	39.75	9.19	87.07	4.44	5.66	4.19
La			1	9.88	45.24	12.42	6.3		53.08	163.96	1.8	33.74	5.79	10.59	4.98
Ce			18.51	133.21	364.98	137.72	99.32		1375.29	1510.76	51.84	444.29	3.84	4.21	3.84
Pr			0.567	5.18	15.02	5.46	3.43		41.96	50.53	1.375	16.8	5.90	11.99	4.99
Nd			2.69	29.07	57.23	29.39	23.14		183.72	192.74	7.45	80.8	5.99	10.78	5.27
Sm			2.23	16.42	48.07	20.77	20.33		86.61	91.09	7.07	49.5	6.84	12.91	6.27
Eu			0.414	0.72	1.64	1.07	0.74		4.49	5.91	0.391	2.66	14.30	27.08	14.00
Gd			8.87	46.16	62.47	74.23	66.42		153.17	224.18	30.03	108.04	4.84	7.13	4.55
Tb			3.74	15.41	27.16	27.98	21.7		60.08	80.83	12.29	39.08	4.00	5.19	3.89
Dy			44.52	177.54	286.99	352.46	272.7		663.54	912.53	152.18	385.31	3.72	4.48	3.71
Ho			17.65	65.57	97.94	135.66	105.61		206.79	302.39	59.71	123.01	3.52	3.96	3.51
Er			90.03	295.72	425.73	640.35	487.86		868.99	1163.7	279.52	497.07	3.34	3.60	3.30
Tm			21.54	63.92	90.82	142.64	101.14		186.66	231.31	61.01	100.4	3.45	3.78	3.42
Yb			233.21	603.22	843.94	1368.77	948.61		1678.71	2012.58	593.75	914.42	3.69	4.25	3.71
Lu			50.47	108.85	125.17	238.1	179.15		252.17	295.85	104.05	141.51	3.32	3.52	3.30
Hf			11471.45	11471.45	12071.82	12483.09	12204.11		13393.82	8534.05	12333.85	8479.79	3.17	3.18	3.17
Ta			0.869	4.28	2.52	11.37	7.13		5.68	8.6	3.29	10.07	4.97	8.33	4.66
Pb			33.11	25.24	45.14	85.5	48.91		50.4	71.86	22.49	51.74	4.29	6.23	4.09
Th			112.28	467.61	324.28	1686.28	912.24		483.19	930.24	491.98	1744.5	3.55	3.80	3.54
U			423.54	937.36	466.05	2782.79	1410.6		1176.73	1161.05	851.3	1353.94	3.30	3.49	3.33
$^{207}Pb/^{206}Pb$			0.2273	0.04605	0.0461	0.0614	0.0590		0.0461	0.0461	0.0550	0.1062			
1σ			0.0134	0.011	0.0071	0.0046	0.0062		0.0294	0.0296	0.0042	0.0094			
$^{207}Pb/^{235}U$			18.7428	0.47015	0.4258	0.6587	0.6328		0.3293	0.3820	0.5861	1.1481			
1σ			1.0530	0.11157	0.0648	0.0474	0.0632		0.2092	0.2443	0.0423	0.0947			
$^{206}Pb/^{238}U$			0.6010	0.07405	0.0671	0.0781	0.0782		0.0519	0.0602	0.0774	0.0785			
1σ			0.0145	0.00209	0.0019	0.0022	0.0030		0.0032	0.0034	0.0021	0.0026			
$^{208}Pb/^{232}Th$			0.1469	0.02382	0.0286	0.0293	0.0297		0.0250	0.0320	0.0265	0.0321			
1σ			0.0267	0.00395	0.0063	0.0069	0.0100		0.0139	0.0133	0.0056	0.0086			
$^{176}Hf/^{177}Hf_m$				0.282595	0.282629	0.282604	0.282649	0.282589	0.282655	0.282545	0.282622	0.282600			
1σ				0.000018	0.000031	0.000015	0.000017	0.000019	0.000033	0.000073	0.000012	0.000015			
$^{176}Lu/^{177}Hf_m$				0.003105	0.001493	0.003866	0.001703	0.003245	0.002687	0.003616	0.001746	0.001761			
$^{176}Yb/^{177}Hf_m$				0.098094	0.060729	0.150997	0.068288	0.103692	0.126253	0.151482	0.063832	0.052047			
$^{206}Pb/^{238}U$ age (Ma)			3034	461	418	485	486		326	377	481	487			
1σ			58	13	11	13	18		20	21	13	16			
$^{176}Hf/^{177}Hf_{i\ (485\ Ma)}$				0.282566	0.282615	0.282568	0.282633	0.282558	0.282630	0.282511	0.282606	0.282583			
εHf				3.75	5.49	3.82	6.13	3.49	6.02	1.81	5.16	4.38			
1σ				0.63	1.09	0.53	0.60	0.67	1.16	2.56	0.42	0.53			

Table 3

Re–Os and Lu–Hf isotope data from Delamerian and Gawler FLIP (and related) A-type systems.

Seismograph Granite Lu/Hf isotope ratios calculated from values in Turner et al. (1992), using Yb/Lu = 4.24 and Zr/Hf = 16.7. GRV Hf and Os data from Fricke (2005). White Hill Hf data from Frost (2009). MGO3009 from Gregory et al. (2008), age from references therein. Seismograph Granite, Black Hill peridotite ages from Turner et al. (1992). Truro Volcanics age from Foden et al. (2002a).

	Cambrian–Ordovician samples						Proterozoic samples					
Name	Marcollat Granite	Mt Monster Porphyry	Seismograph Granite	Black Hill peridotite	Truro Volcanic	Truro Volcanic	Sybella Granite	Sybella Granite	Chitanilga	Roopena	Roopena	White Hill
Sample #	PG11-2727	2001	2000		876–1013	876–1013 (dup)	7820–5068	MGO3009	C-CH-16	697440	697443	WTH101
Age (Ma)	480 ± 2.5	485 ± 7.9	490	490	522	522	1560	1560	1592	1592	1592	1592
Os (ppb)	0.000800	0.000518	0.000211	0.405300	0.017642	0.018190	0.001700	0.001400	0.115700	0.145000	0.098000	0.011800
2σ	0.0000100	0.0000026	0.0000011	0.0020265	0.0000882	0.0000909	0.0000085	0.0000070	0.0005785	0.0007250	0.0004900	0.0000500
Re (ppb)	0.00125	0.00350	0.00101	0.17983	0.02144	0.02144	0.01044	0.01373	0.82515	0.83689	0.47645	0.02076
2σ	0.00002	0.00005	0.00002	0.00270	0.00032	0.00032	0.00016	0.00021	0.01238	0.01255	0.00715	0.00031
$^{187}Os/^{188}Os_m$	0.268857	0.82521	0.58663	0.242445	0.23431	0.23786	6.31870	3.83774	18.89474	6.74690	8.77818	1.567800
2σ	0.000670	0.01	0.01	0.000360	0	0	1.1634	0.02	0.03	0.06	0.01	0.004420
$^{187}Re/^{188}Os_m$	19.19	85.73	56.41	5.46	5.93	5.76	53.40	70.10	118.50	51.80	49.80	23.13
1σ	0.37	1.36	0.89	0.09	0.09	0.09	0.84	1.11	1.87	0.82	0.79	0.36
$^{187}Os/^{188}Os_i$	0.114813	0.129723	0.105155	0.197673	0.182511	0.187547	4.912663	2.036327	15.709744	5.354639	7.439681	0.946996

	In-situ zircon			In-situ zircon			Whole rock				
	Max	Min	Average	Max	Min	Average	Seismograph Granite	Chitanilga	Roopena	Roopena	White Hill
Hf (ppm)							15.0	5.91	4.00	4.23	0.07
Lu							1.5	0.53	0.49	0.50	0.03
$^{176}Hf/^{177}Hfm$	0.282776	0.282544	0.282603	0.282986	0.282525	0.282652	0.282701	0.282168	0.282356	0.282397	0.283533
1σ	0.000028	0.000020		0.000036	0.000066		0.000020	0.000011	0.000011	0.000020	0.000033
$^{176}Lu/^{177}Hf_m$	0.002008	0.000608		0.003142	0.006677		0.013925	0.015400	0.017405	0.016699	0.057683
$^{176}Hf/^{177}Hf_i$	0.282757	0.282538	0.282590	0.282956	0.282462	0.282625	0.282569	0.281687	0.281813	0.281875	0.281733
εHf (t)	10.42	2.67	4.50	17.58	0.09	5.74	3.97	−1.73	2.73	4.95	−0.10
1σ	0.49	0.35		0.63	1.16		0.71	0.40	0.37	0.69	1.16